

Optimization of Modeling and Simulation of Explosively formed Projectiles through Water



By

Munir Ahmad

School of Chemical and Materials Engineering,
National University of Sciences and Technology

2014

Optimization of Modeling and Simulation of Explosively formed Projectiles through Water



Name: **Munir Ahmad**
Reg. No: **2010-NUST-MS PhD-E-11**

(This work is submitted as an MS thesis in partial fulfillment of the requirements for the degree of MS in Materials and Surface Engineering)

Supervisor Name: Dr. Mohammad Mujahid

Co-Supervisor Name: Dr. Arshad Hussain

**School of Chemical and Materials Engineering (SCME),
National University of Sciences and Technology (NUST),
Islamabad, Pakistan**

August, 2014

Certificate

This is to certify that work in this thesis has been carried out by **Mr. Munir Ahmad** and completed under my supervision in simulations laboratory, school of chemical and materials engineering, National University of Sciences and Technology, H-12, Islamabad, Pakistan.

Supervisor: _____

Dr. Mohammad Mujahid

Co-supervisor _____

Dr. Arshad Hussain

Principal/ Dean HOD Chemical Engineering

School of Chemical & Materials Engineering

National University of Sciences and Technology, Islamabad

Submitted through

Principal/Dean,

Materials Engineering Department

National University of Sciences and Technology, Islamabad

DEDICATED

To

My parents, wife & kids, sisters & brothers

Acknowledgements

All praises are due to Almighty Allah who gave me the strength, wisdom, ability and the opportunity to work on this project.

I would like to offer my sincerest and deepest thanks to my supervisors Dr. Muhammad Mujahid and Dr. Arshad Hussain for giving me the opportunity to work with them and for their kind and dynamic supervision throughout this project. Their guidance and valuable suggestions resulted in the successful completion of this project.

I am grateful to Ms. Shadab Kamal, Mr. Abdul Hamid, Mr. Syed Tanweer Hasan , and Mr. Ziaullah , for their guidance and encouragements.

I am very much thankful to Mr. Faisal Hameed for his conceptual discussions and all kind of support.

I am very much thankful to Dr. Muhammad Asim, Dr. Aamer Habib, Dr.A.Q.Malik, Dr. Ghulam Hussain, Mr. Saleem Tahir, Mr. Abid Farooq , Dr. Fayyaz Hussain Asghar , Mr Mukhtar Ahmed Gondal , Dr. Asad Ahmed, Mr. Faizullah, Mr. Sarfraz Ahmed, Dr. Manzoor Ahmed, Dr.Qaisar Abbas, and Dr. G.S.Naz for their conceptual help and encouragement.

I wish to express my feelings of gratitude for my parents and family, who have always been a source of encouragement, guidance and prayers for me.

Abstract

This project report describes a numerical modeling of explosively formed projectiles (EFP) passing through void and water. Explosively formed projectiles are being used for neutralizing sea mines. Penetration through water is studied by using copper, and Tungsten made liners. Copper made liners show poor performance in water as they eroded immediately on passing through water; however their length of penetration can be extended to some extent by changing liner thickness (contour type thickness) and by making solid final shape. Their penetration length can also be increased by replacing copper with tungsten from 4 to 8 times. Liner curvature is very sensitive parameter to its final shape and velocity. In this report a good exercise is done by varying liner curvature and optimum curvature for that particular design ($\theta=120^\circ$) is obtained. Effect of moving water on EFP performance is also studied and it is concluded that if water is moving in opposite direction, with normal river speed, then it has no pronounced effect on the EFP performance. Of all the available explosives HMX shows better results as it has higher density and detonation velocity. EFP devices are similar to a shaped charge, except the apex angle of the liner, which is greater than or equal to 120° (depending upon material used). EFPs are low-velocity devices as compared to shaped charges and have a tip velocity of 2-3 km/s (7-12km/s in case of shaped charges). However, they generate large diameter, high mass projectiles and produce large holes in the target material.

Underwater mines clearance is a difficult and demanding task. Under water munitions cannot be defused, neutralized or transported to any other places. If the velocity of explosively formed projectile (EFP) is low enough and the hole it creates in the casing of the underwater munitions is large enough, explosive charge contained in it will burn without detonation thus ensuring that mine has safely defused.

Table of Contents

List of Tables	xii
List of Figures	xiii
INTRODUCTION	1
Chapter 1: EFPs and Sea-mine Neutralization.....	4
1.1 Hydrocode Modeling and Simulation Scheme	5
Chapter 2: Conventional Devices	6
2.1 Kinetic Energy devices	6
2.2 Chemical Energy devices.....	6
2.2.1 Omni Directional Chemical Energy Devices.....	7
2.2.2 Directed Energy Chemical Energy Devices	7
2.2.1 Omni Directional Chemical Energy Devices.....	7
2.2.1.1. Fragmentation	7
2.2.1.2. Blast	8
2.2.2. Directed Energy Chemical Energy Devices	8
2.2.2.1 High Explosive Squash Head (HESH) Devices.....	8
2.2.2.2 Shaped Charges.....	9
2.2.2.3 Jet Projectile Charges (JPC).....	10
2.2.2.4 Explosively Formed Projectile (EFP)	11

Chapter 3	Characteristics of Explosively Formed Projectiles and their penetration in the target	12
3.1	Origin of EFPs	12
3.2	Mechanics of EFP Formation	14
3.3	Formation Process of EFP	16
3.4	Major Components.....	17
3.5	Different Shapes and Forms of EFPs.....	18
3.6	Parameters Affecting the EFP Characteristics.....	19
3.6.1	Geometrical Factors	19
3.6.2	Liner Geometry	20
3.6.3	Case Confinement.....	21
3.6.4	Explosive Configurations.....	21
3.6.5	Explosive Initiation Technique	21
3.6.6	Detonation Wave and final shape	22
3.7	Material Factors	23
3.7.1	Liner material.....	23
3.7.2	Casing material	23
3.7.3	Explosive material	23
3.8	Processing Conditions of Liner.....	24
3.9	Standoff.....	24
3.10	Uses of EFP.....	25
3.11	Penetration	25

3.11.1	Mechanisms for defeating armor	25
3.11.2	Long rod warhead penetration	26
3.11.3	Shaped charges jet warhead penetration	26
3.11.4	EFP warhead Penetration	26
3.12	Conclusion	28
Chapter 4	System of Governing equations and solution techniques for Explosive Metal Interactions	29
4.1	Introduction.....	29
4.2	Explosive Metal Interaction.....	30
4.3	Low and High Velocity Phenomenon.....	31
4.3.1	Structural dynamic problems	32
4.3.2	Impact or wave propagation problems.....	32
4.4	The Governing Equations	33
4.4.1	Kinematics	33
4.4.2	Conservation Equations	34
4.4.2.1	Conservation of Mass	34
4.4.2.2	Conservation of Momentum	35
4.4.2.3	Conservation of Energy	35
4.4.3	Jump Equations.....	36
4.4.4	Constitutive Equations.....	37
4.5	Numerical Methods and Solution Techniques.....	39
4.5.1	Important Concepts in Numerical Simulations.....	40

4.5.1.1 The Finite Element Method	40
4.5.1.2 The Finite Difference Method	40
4.5.1.3 The Finite Volume Method.....	41
4.5.2 Problem Formulation Techniques.....	41
4.5.2.1 Lagrangian formulation	42
4.5.2.2 Eulerian formulation	43
4.5.2.3 Advantages and disadvantages of Lagrange and Euler formulation.....	43
4.5.2.4 ALE (Arbitrary Lagrangian-Euler)	43
4.5.2.5 SPH (Smooth Particle Hydrodynamics) formulation	44
4.5.2.6 Molecular Dynamics	44
4.5.3 Equation of State (EOS).....	45
4.5.3.1 Ideal Gas equation of states	46
4.5.3.2 Noble Able equation of states	46
4.5.3.3 Tait Equation of State	46
4.5.3.4 BKW Equation of State	46
4.5.3.5 JWL Equation of State	47
4.5.3.6 Mie Gruneisen Equation of State.....	47
4.5.4 Hydrocodes	48
4.5.4.1 AUTODYN.....	48
4.6 Conclusion	49

Chapter 5 Results and Discussion.....	50
5.1 Design 1[25].....	50
5.1.1 Conclusion:	52
5.1.2 Conclusion:	53
5.1.3 Conclusion	53
5.2 Design 2	53
5.3 Design 3	57
5.3.1 Conclusion:	58
5.4 Design 4 (dumpling)	59
5.5 Design 5 (Final Heart shape)	62
5.6 DESIGN 6	64
5.7 Effect of moving water on EFP performance	70
5.8 Summary and conclusions	72
5.9 recommendations	72
References	73

List of Tables

Table 5.1: Design parts and their EOS and Material Models,	51
Table 5.2: Comparison of Experimental and Simulation Results for Design 1	.52
Table 5.3: Design parts and their EOS and Material Models,	57
Table 5.4: Effects of Liner curvature on EFP performance	66
Table 5.5 comparison of penetration distance in water when EFP has velocity 0.55km/s.....	68
Table 5.6: Effects of different explosives on EFP shape, velocity and L/D Ratio	69

List of Figures

Figure 2.1: Classification of warheads	7
Figure 2.2: High Explosive Squash Head Device	9
Figure 2.3: Shaped charge components.....	10
Figure 2.4: EFP on the way to its flight.....	11
Figure 3.1: comparison between shaped charge and EFP	12
Figure 3.2: Liner collapse in shaped charge.....	14
Figure 3.3: slug and jet velocity as a function of cone angle	14
Figure 3.4: Elements of EFP Liner under the influence of explosive	15
Figure 3.5: components of EFP	16
Figure 3.6: Taper casing and cylindrical casing.....	18
Figure 3.7: Forward, Backward and W Fold EFPs	20
Figure 3.8: Explosive type and projectile shape.....	22
Figure 4.0: pressure-distance plots.....	31
Figure 4.1: Different positions of an object.....	33
Figure 4.2: lagrange mesh deformation.....	42
Figure 5.1: Initial stage of design 1	50
Figure 5.3: Simulation results for copper and Iron at reference times.	52
Figure 5.4: Comparison of target penetration cross-section produced by Fe EFP.	52
Figure 5.5: Comparison of target penetration cross-section produced by Cu EFP.	53
Figure 5.6 Initial stage of design 2	53
Figure 5.7 Simulation done by C. Lam at time 0 20 30 50 70 and 100 μ sec [24]	54
Figure 5.8 Experiments taken snapshots at time 50, 70, 100 μ sec [24]	54
Figure 5.9: simulation done at time 20 30 50 70 and 100 μ sec.....	54

Figure 5.11: Elongated EFP passing through water at times 110, 120, 140, 150,160, 180,190, 210 and 230 μ sec	55
Figure 5.12 Experiments taken snapshots at time 120, 150 μ sec [24]	55
Figure 5.13: Elongated EFP passing through water simulation results at times 120 150 μ sec [24].....	56
Figure 5.14: Elongated EFP passing through water	56
Figure 5.14: Initial Design 3.....	57
Figure 5.16: Velocity profile of EFP in water design 3	58
Figure 5.17: Velocity profile of EFP in void water design 3	58
Figure 5.17a: W-shaped EFP on the way in void and water at 40, 60, 80,100,200,400,662 μ sec	59
Figure 5.18: dumpling EFP at times 60, 90 and 150 μ sec[24].....	59
Figure 5.20: dumpling EFP through water	60
Figure 5.21: dumpling EFP [24].....	61
Figure 5.22: shapes of dumpling EFP in water	61
Figure 5.23: dumpling EFP Velocity profile in void and in water.....	62
Figure 5.24: Heart EFP formation steps at 10 20 30 40 50 and 60 μ sec.....	62
Figure 5.26: Heart EFP Velocity profile in void and in water	63
Figure 5.27: Heart EFP Velocity profile in water	64
Figure 5.28: formation of Tungsten EFP in void	64
Figure 5.30: formation of Tungsten EFP in Water.....	65
Figure 5.31: Optimization of curvature of Tungsten-EFP in water.....	66
Figure 5.32: Velocity profile of optimized Tungsten-EFP in water.....	67
Figure 5.33: Velocity profile of optimized Tungsten-EFP in water.....	67

Figure 5.34: Behavior of velocity of water on Tungsten EFP penetration in water70

Figure 5.35: Effect of velocity of water on Tungsten EFP penetration in water...71

INTRODUCTION

An explosively formed projectile (EFP) devices are like shaped charges, apex angle separate these two categories of devices. For EFP it is greater than 120° greater. EFPs typically are low-velocity devices (as compared to shaped charges) and have a velocity of 2-3 km/s. However, they generate large diameter, high mass projectiles and produce large holes in the target material.

Under water mines clearance, are cumbersome and of demanding task. Underwater munitions in many cases cannot be defused, neutralized or transported to any other places for their destruction, and the only way out may be their destruction by detonation in situ. For large munitions, this involves a great risk of severe damage to the surroundings, so a less hazardous procedure would be desirable. If the velocity of explosively formed projectile (EFP) is low enough and the hole it creates in the casing of the underwater munitions is large enough, a burn out of explosive charge contained in it without detonation or deflagration may ensure.

Detonation initiations conditions for various explosives for EFPs and shaped charges have been studied by Chick et al in 1981, 1989[19, 20]. The optimized critical velocity of jet to cause initiation of detonation of the explosive of the sea mine is dependent on several factors, one of which is the presence of the casing. The casing can reduce the sensitivity of the penetrator due to the pre-compression of explosive contained by the formation of the critical pressure wave. If the velocity of the EFP is less than the critical value, the phenomenon of detonation will not occur.

As the jets or the EFPs passes through the water their temperature becomes lowered and the hot remnant of the shaped charges and an EFP can cause low order burning in the explosive. If there is less or no chance of escaping the combustion products, the pressure builds up and can cause deflagration. If the munitions is under ground or located underwater, the damage may be quite severe. Especially in case of underwater greater energy goes into the bubble pulses than in case of detonation. When the explosive charge

detonates, it is instantaneously converted into gas. The produced gas at extremely high temperature at first occupies the same volume as that of the explosive. The pressure of the suddenly produced gasses products is so high and creates bubbles which will have an internal pressure of 20% of the detonation pressure of explosive, of the order of 5 Giga Pascal (G pa).

It is therefore required to design a suitable device that can cause the low order burning and creates relatively large hole in the munitions casings to allow the escape of the combustion products. The escape of the gaseous products avoids the pressure build up and resulting in violent deflagration. EFPs offer a possible solution to this problem.

Here, our main interest is to find out the effective use of an EFP as a stand-off sea mine device for underwater mine neutralization. The device should neutralize underwater munitions in low water without detonating them. The standard EFP produces a relatively thin projectile, which erodes rapidly and is thus unsuitable for the task. An ideal EFP should possess sufficient mass to reduce the effect of erosion, a large diameter hole to create in the casing of sea mine for high pressure gas venting and a relatively low velocity to prevent excessive shock transmitted to the explosive of sea mine on impact.

Penetration behavior of explosively formed projectiles (EFP) passing through water is of great military significance of use, although very few investigations have been reported in this aspect. We must realize that the water will behave as a target or as a part of the target having density of 1000 Kg. m⁻³ that causes the projectile slowing down and is being eroded as it passes through water. This effect has been shown for fast moving shaped charge jets by Zernow in 1987 [22] in their study of soft capture of shaped charge jet particles using low density foamed liquids. The study of the performance of EFPs in water by Janzon (1993) [23] investigated that EFPs fired at high velocities, greater than 1700 ms⁻¹, were decelerated faster than that of with lesser initial velocities. At penetration greater than 100 mm (1.6 CD), the EFPs with the higher initial velocities actually had lower velocities than did EFPs with lower initial velocities. They also showed that the head of the EFP was eroded and subsequently penetration was stopped when water entered the hollow core of the projectile. For increased penetration in water it

is necessary to form a solid projectile rather than the hollow one. This would be done by changing the liner geometry, liner material and the confinement.

EFP formation process depends on liner apex angle and mass distribution of the liner if EFP configuration including parameters like liner thickness, outer casing, explosive, liner material etc. remains same. When we consider use of an explosively formed projectile for under water applications, the interaction b/w water and the EFPs is an important feature to consider. As the water behaves like small density armour or a part of the target for high speed projectiles, the efficiency of the formed projectile in water can be significantly reduced. Numerical simulation is performed in order to draw as well as optimized EFPs design and its penetration

EFP design has in the past dependent on an experimental trial and error methods and the lack of reliable finite element, volume and difference codes. The designs at start were expensive and time consuming. The presence of different finite element, volume and difference codes called hydrocodes now made the design of different problem in this regard easy and cost effective. The Dyna2D hydrocode is one among many codes developed to make the work more efficient and cost effective. This report describes the application Autodyn 2D finite element Code to numerically model the formation and penetration of the projectile formed in water and the experimental verification of the model with flash radiography.

The main object of any missile or projectile is to damage a target to a considerable extent. An EFP is potentially used because it is an effective way of increasing the amount of damaging energy obtainable to the system at the time of engagement and it improves the coupling of the energy to the target. It also allows the destructive effect to be better matched to the likely response of the target (it gives a choice of lethal mechanism) [14].

Chapter 1: EFPs and Sea-mine Neutralization

Underwater mines are a huge threat to oceanic life. Their elimination by transportation or neutralization is not safe neither easy. These mines are very sensitive and their handling is also very critical. We have to avoid detonation rather we prefer burning of the explosive. In burning combustion reaction rate is subsonic, in detonation combustion reaction rate are supersonic. So we prefer burning instead of detonation

Under-water mines can be defused by using either an EFP or a shaped charge projectile. Disposal of both expired and unexploded weaponry having highly sensitive nitro-methane formulation by using shaped charge jet has been examined in [26]. High explosive can either be deflagrated or exploded by tuning the jet-tip geometry [27]. It also depends on critical energy which in turn related to the ratio of jet tip velocity to its diameter. Therefore an EFP, owing to its configuration, conveys suitable amount of energy to cause deflagration and avoids detonation.

An EFP or shaped charge jet has to penetrate through water and underwater mine's casing before transmitting its remaining energy to the explosive contents. In this condition, water acts as a target material having density 1.0g/cm^3 . Jet penetration through foam liquid having low density has been inspected to obtain jet structure data using "soft" jet recovery technique and flash x-ray diffraction by Zernow et al [3]. By using this structure data kinetic energy density of the shaped charge jet can be calculated at any time. Faster EFPs are retarded faster than those having smaller initial velocities. this effect of EFPs is studied by Janzon et al in 1993 [23]. Effect of critical energy has been studied by Walker et al. He confirmed that encased explosive requires critical energy (V^2/d) to initiate [28]. Where 'V' is the jet velocity and 'd' is the jet diameter. Effect of critical power density has been studied by Lee et al. He confirmed that the critical power density to detonate the explosive charge is equivalent to V^3/d [29]. They both concluded that comparatively low velocity and having jet with large diameter is desirable for deflagration.

As explained above the critical energy density of the shaped charge jet depends upon its tip velocity and diameter. A smaller tip dimension is the indications of high kinetic energy density which leads to detonation, moreover small dimension diameter in the underwater mine's casing does not allow the gaseous products to escape and hence detonation process occurs. Thus for deflagration a slower jet tip velocity with larger diameter of the jet is required. Thus EFP configuration is more suitable. Thus an EFP which have these two qualities and an additional large standoff is the best candidate for underwater mine's clearance.

Initiation conditions for detonation of different kinds of explosives by EFPs and shaped charge jets have been investigated by Chick et al in 1981, 1989 [19]. The critical energy density of a jet to cause detonation of the explosive in underwater munitions is dependent on several factors including EFP diameter, material, standoff, casing material, casing thickness etc.

The effective use of an EFP as a stand-off underwater mine's clearance has been investigated in the present study. Liner Material optimization is done for better penetration and at the same time to meet the other parameters requirements for deflagration.

1.1 HYDROCODE MODELING AND SIMULATION SCHEME

The experimental cost of an underwater mine's neutralization is very high. Many hydro codes has been developed for the simulation of EFPs and shaped charges. With the help of these codes cost and time saved. AUTODYNE is one of them. Here this code is used to study the effect of EFPs and shaped charges numerically [30]. The formation and efficiency of the EFPs have been judged by using this code. The AUTODYN uses both Lagrangian and Euler techniques. The AUTODYN is an efficient code as reported in the literature. In this work ANSYS AUTODYN-2D V 12.0 has been used for the optimization of EFPs through the water.

Chapter 2: Conventional Devices

The part of arming system used to destroy or damaging the enemies territory is called a warhead. Conventional warheads are of two types

- a) Kinetic Energy devices
- b) Chemical Energy devices

2.1 KINETIC ENERGY DEVICES

In these devices the propellant is used to accelerate the metallic plate often called projectile to a very high velocity [2]. The main purpose of a warhead device is to damage the target. The destruction is possible only when there are excessive stress on the target structure, and consequently failure of the target structure. The amount of energy which is transferred into the target causes the damage or Behind Armor Effects (BAE). These are old devices used to defeat armored targets .It remains the most important system for a long time. Modern KE projectile can trace their roots to the armor piercing shot developed by Palliser to attack iron clad ships in the 1860s. Today most KE projectiles contain no explosive charge, but rely on other mechanisms to inflict damage on the targets. All forms of KE attack rely on imparting sufficient energy to a penetrator so that at the end of its trajectory it has enough residual energy to overmatch the target and penetrate and still cause damage within the tank. The KE devices will usually use materials with high density and a high length to diameter ratio. Consequently maximize the KE density at target. Example of KE warheads are rigid and non-rigid Armor Piercing Composite Rigid (APCR) projectiles, etc. [14].

2.2 CHEMICAL ENERGY DEVICES

In these devices explosives energy is used for the destruction of the target by accelerating the metal to form EFP or shaped charge or simply blast. The family of high explosives, conventional warheads is divided into two main categories as depicted in the classification chart figure 2.1 [2].

2.2.1 Omni Directional Chemical Energy Devices

2.2.2 Directed Energy Chemical Energy Devices

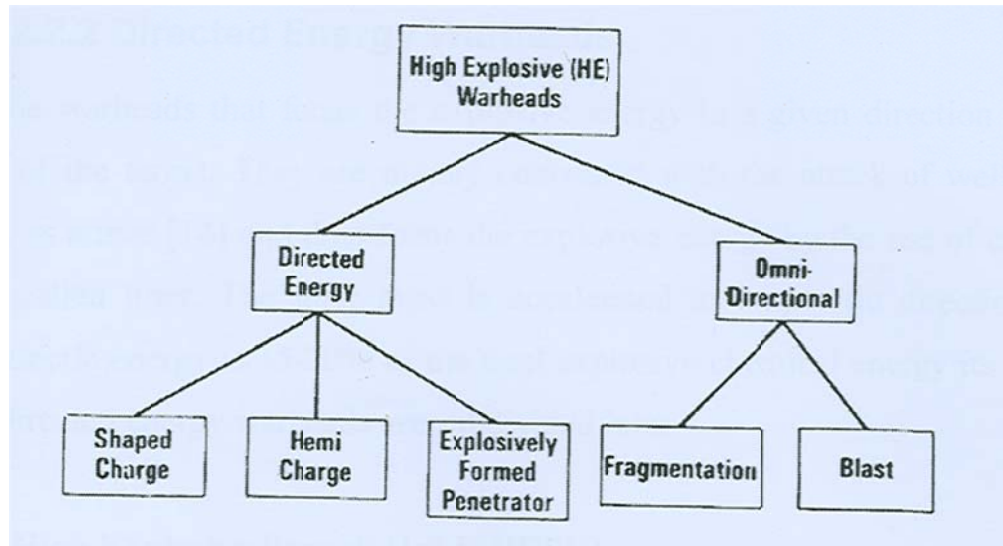


Figure 2.1: Classification of warheads

2.2.1 Omni Directional Chemical Energy Devices

These are the devices in which Destruction is caused in 4π geometry. After detonation, the explosive quickly spread in all directions and the casing of the device broken into piece with velocities of the order of 1700m.s.these devices have their own advantages and disadvantage. These devices cause Damage up to a limited distance.

2.2.1.1. Fragmentation

As it clear from the name that the casing broken into pieces called projectiles, These projectiles uses the energy of the explosive and causes the damage to the target.

2.2.1.2. Blast

In blast no metal pieces it is only the shock wave pressure that causes the destruction to the target. [2].it is the cheapest and the simplest explosive device. Its strength lies in the strength of shock wave produced by the detonation of the explosive. [14].These devices also cause Damage up to a limited distance.

2.2.2. Directed Energy Chemical Energy Devices

In these devices the explosive energy is focused into one direction so that maximum penetration can be achieved. They are used for the attack on armor [14] and energy of the explosive is focused on a cavity called liner. The liner is shaped and accelerated to a specific direction and the amount of kinetic energy is 15-20% of the total explosive chemical energy its way to the target [2]. Directed energy devices are subdivided into:

2.2.2.1 High Explosive Squash Head (HESH) Devices

It is the unidirectional energy warhead type device. Its principle is shown in figure 2.2. it is used against building and tank armor.it is also used against modern era armors, such as spaced armor, composite armors and explosive reactor armor (ERA), it is much less effective as a guided weapon warhead it has been superseded. large amount of explosive is used in it for operation of the device. These are very heavy weight so transportation at the target is a bit issue.

When explosive mass is detonated shock waves are produced. These shock waves travel towards the metal plate and passes through it as a compressive waves. These waves when reaches the other end of the plate there is a medium change. Some part of the wave reflected from the rear side of the plate as a tensile wave.at a point where compression and tensile wave intersect a huge stress zone is created so a scab of material is detached as shown in figure 2.2 having velocity range of 100-250 m/s. [14].

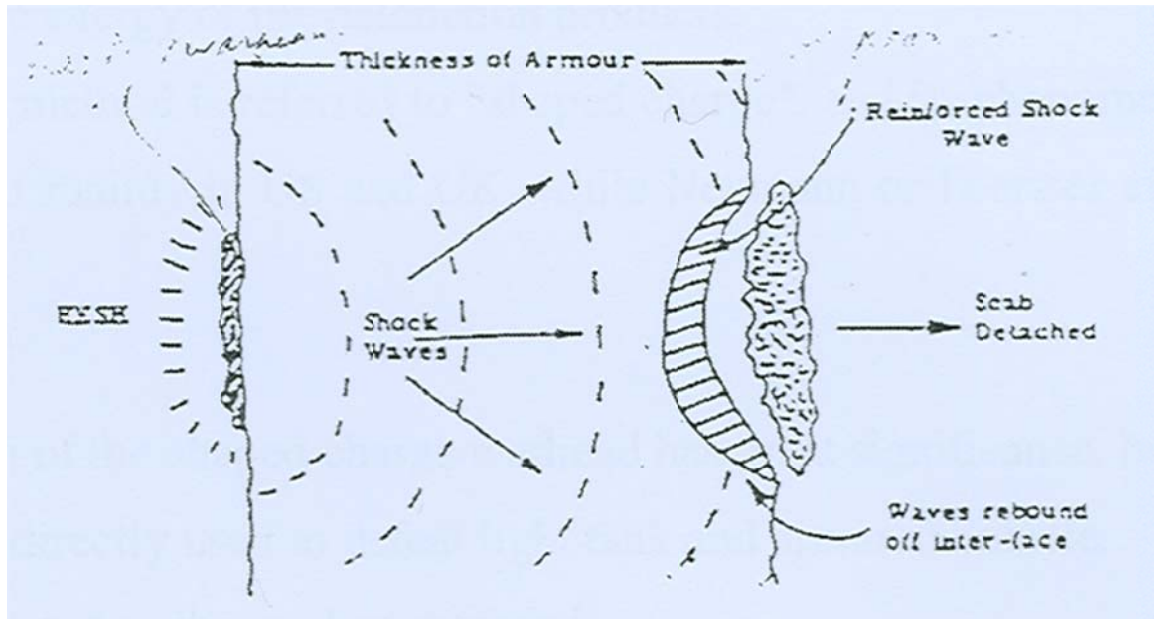


Figure 2.2: High Explosive Squash Head Device

2.2.2.2 Shaped Charges

A typical shaped charge warhead is depicted in figure 2.3. there application field become broader and broader with the passage of time. Liner is often conical shaped with apex angle of less than or equal to 120° . In world war 2nd it was first used. Very small stand-off as compared to EFPs, having very large penetrating length as compared to EFPs. Shaped charges have small caliber of perforation. In 1970s, EFPs are developed having large caliber of damage in the target .EFPs have very good secondary effects and also have no effect of air on them. [15j].

A cylinder of high explosive having a hollow cavity in one end and a detonator at the other end is used to obtain very high velocity metal jet (12 km/s). The hollow cavity is often conical shape type and is called, “liner”, . The gaseous products are produced after detonation producing high pressure in a very small region. This pressure forces the liner material to reshape and accelerate to about 10 to 12 km/s.

This acceleration method is referred to “shaped charge”, and its phenomenon is known as the Munroe effect mainly in US and UK, while Neumann or Forester effect in the other countries [16].

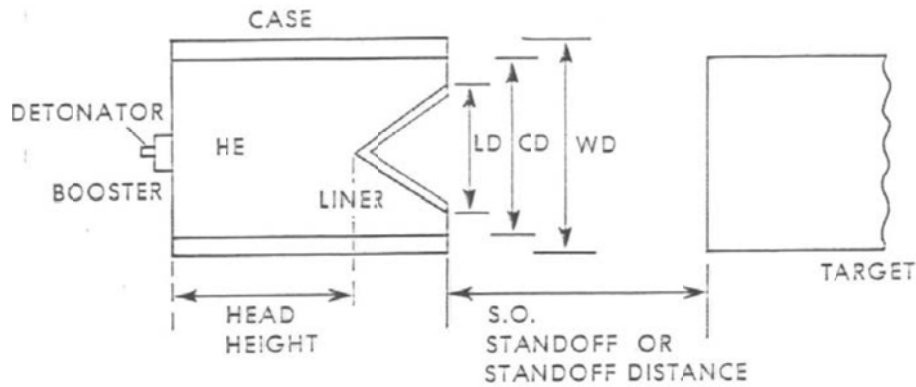


Figure 2.3: Shaped charge components

The research of the shaped charge warhead has great significance, and its application areas are as under

- (1) Defeating light tank
- (2) Defeating armored vehicles
- (3) Used to the tandem warhead.
- (4) For defeating the ERA
- (5) Holding up of guided missile
- (6) In the field of space flight facilities.
- (7) Drilling under the bad circumstances of engineering blast.
- (8) Oil-well drilling industry.

2.2.2.3 Jet Projectile Charges (JPC)

It is used for concrete material to break. JPC is a new type for blasting the targets. It has velocity gradient of about 3-5mm/s between jet and rest of the slug. Copper can be used as the liner. [17].

2.2.2.4 Explosively Formed Projectile (EFP)

It produces a high mass rod or fragment of moderate velocity (typically 1.5-3 km/s) as depicted in figure 2.4, and following section it is described in details.

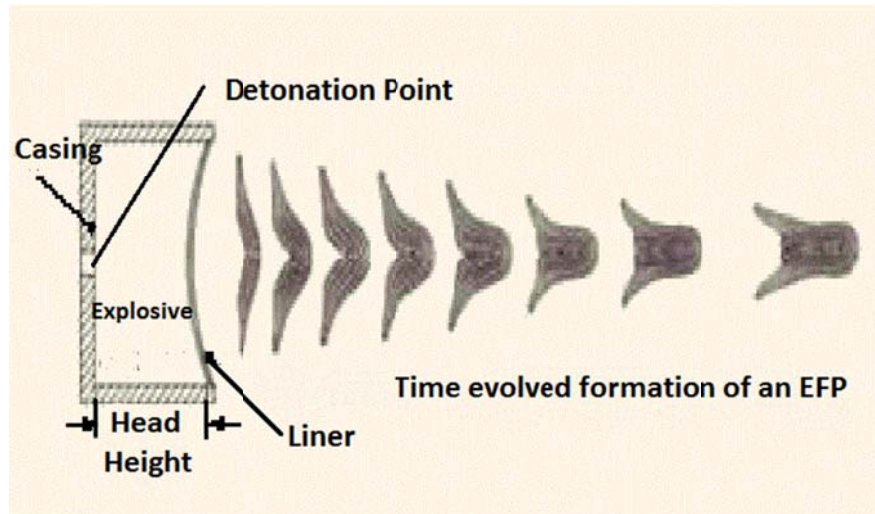


Figure 2.4: EFP on the way to its flight

Chapter 3 Characteristics of Explosively Formed Projectiles and their penetration in the target

3.1 ORIGIN OF EFPs

The concept of using explosive energy to deform a metal plate into a coherent penetrator while simultaneously accelerating it to extremely high velocities offers a unique method of employing a kinetic energy penetrator without use of a large gun. However, the concept was primarily used in mines until the mid-1970s when top attack systems capable of standing off from the target and addressing the more vulnerable target tops were introduced. The explosively formed projectile (EFP) is a natural warhead selection for these systems. This chapter will point out that many differently shaped projectiles can be formed, and warheads can be sized to fit most weapon systems [2].

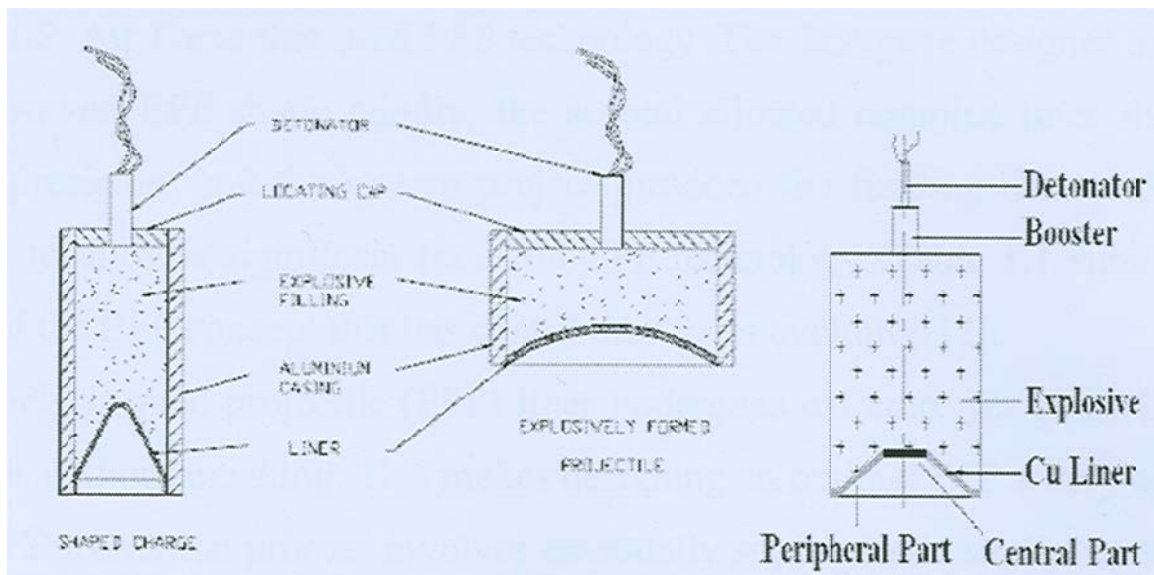


Figure 3.1: comparison between shaped charge and EFP

A typical EFP warhead is shown in figure 3.1. Also known as an explosively formed penetrator, self-forging fragment, Misznay-Schardin charge, mass focus device,

and the P-charge, the EFP warhead is made up of a metallic liner and case, an explosive section and an initiation train. Very often there is also a retaining ring to position and hold the liner-explosive subassembly in place. After detonation, the explosive products create enormous pressures that accelerate the liner while simultaneously reshaping it into a rod or some other desired shape. The EFP then hits the target at speeds in excess of 2000 m/s, delivering billions of watts of mechanical power [2].

The idea of EFP is not new one .in 1936 R. W. Wood designed an experiment by using some detonators with shallow cavities in the explosives. Copper liner is used at the cavities ends. Wood explained that when detonation occurs, copper in each cavity formed a pellet that was projected at a very high velocity and that traveled long distances in a coherent fashion. The explosive formation of a projectile later became known as the Mischay-Schardin effect. Mischay demonstrated this effect in Germany with a 400-mm diameter charge and a 300-mm diameter iron liner in July 1944 [2].

During the early 1970s, EFP technology escalated significantly, primarily because of three simultaneous developments: 1)the success of hydrocode simulation techniques to model EFP device, 2) the progress in high precision computer numerical control (CNC) manufacturing techniques and 3) a number of system concepts sponsored by both the US Army and U.S. Air Force that used EFP technology. The first gave designer the ability to achieve improved EFP shape rapidly, the second allowed complex liner shapes to be made with precision, and the system project provided the funding base and a specific requirement to allow a significant focus on EFP technology.

The final shape and velocity of an explosively formed projectile (EFP) is very sensitive to its initial parameters. EFP undergoes very high plastic deformation. So the design of optimum EFP is therefore very complicated. The process of formation of an EFP comprises essentially super plastic strains up to 300%, at strain rates of the order of 10^4 per second, with a resulting adiabatic temperature rise of up to 1000k or more. Conventional theories cannot explain such type of super plastic behavior that only use dislocation generation and arrangements to accommodate strain [10].

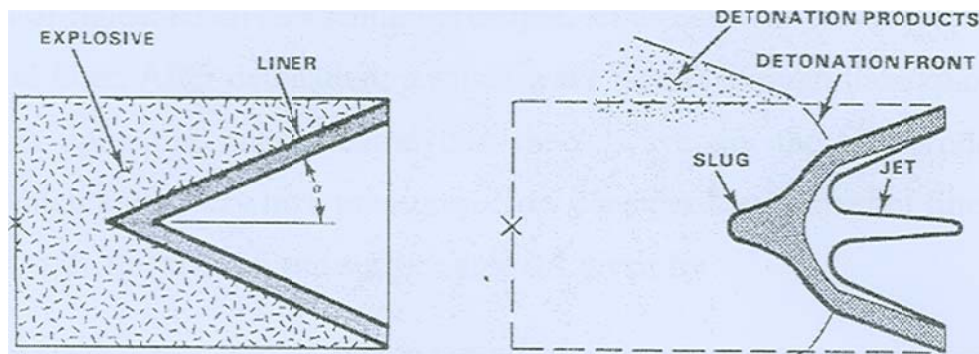


Figure 3.2: Liner collapse in shaped charge

3.2 MECHANICS OF EFP FORMATION

To place the EFP technology in perspective, it is helpful to examine its liner collapse in the context of the more familiar shaped charge warhead. A shaped charge is an explosive device that has a deep metal lined cavity that is typically conical. As shown in figure 3.2, the shaped charge liner normally splits into a very fast jet and a much slower moving slug, which eventually separate from each other. The jet makes up about 15% of the liner mass, and the rest remains in the slug. As the half cone angle is increased, the inward collapse becomes less violent and there is correspondingly less of a velocity difference between the jet and slug. In fact, as shown in figure 3.3, it was found that as the half cone angle approaching 75 degree, the jet and slug approach the same velocity and become indistinguishable. Hence at these angles, an EFP is formed [2].

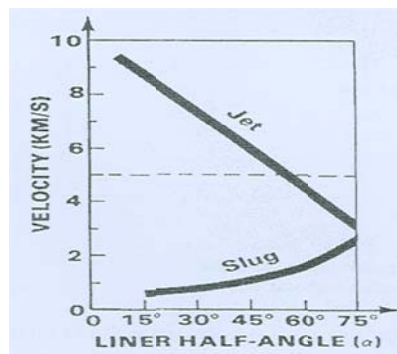


Figure 3.3: slug and jet velocity as a function of cone angle

On the basis of fundamental momentum principle, let us consider the interaction between explosive and liner. After detonation, a shock wave passes through the explosive charge and impinges upon the liner. Behind this shock wave are the gas products of the explosion, which are at very high pressures. Now consider the element of liner, with thickness h and surface area dA given by

$$dA = r_\theta r_\phi n d_\theta d_\phi$$

Where r_ϕ and r_θ are the local radii of the curvature of the element and n is its unit normal vector. As the shock wave passes over this element, the gaseous products push on this element with a pressure $p = p(t)$, causing the element to accelerate. The total time of the effective interaction results in an impulse P that is delivered to the liner element causing it to attain a final velocity V or

$$P = \int p dA dt = V dm$$

Where ($dm = \rho h dA n$) is the element's mass. Let us consider axisymmetric or two dimensional liner surfaces. The fundamental rules that will be established will also apply, or can easily be extended, to three dimensional liners as well.

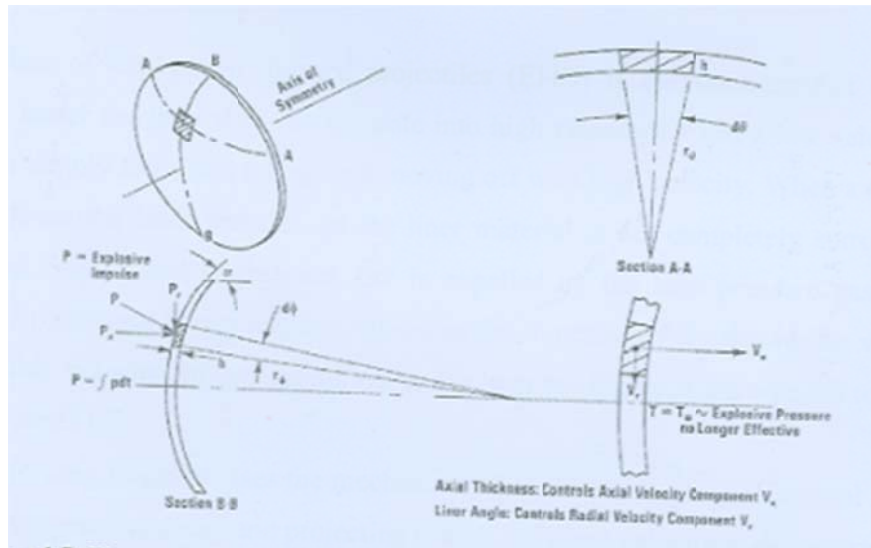


Figure 3.4: Elements of EFP Liner under the influence of explosive

The fundamental vectors can then be written in component form as:

$$P = P_x i + P_r j$$

$$V = V_x i + V_r j$$

$$n = i \cos \alpha + j \cos \beta$$

Where r and x represent the radial and axial components and i and j are the unit vectors in the x and r direction, respectively. The individual velocity components are, therefore, given by

$$V_x = P \sin \alpha / \rho h d A$$

$$V_r = P \cos \beta / \rho h d A$$

The final mapping of all of the liner elements, that is, the final EFP shape, is governed by the distribution of these velocity components along the liner.

Therefore, given an initial liner configuration that produces a certain EFP shape, one can modify the liner and produces a different or modified shape by changing the liner angle α and thickness h in accordance with Equations given above [2].

3.3 FORMATION PROCESS OF EFP

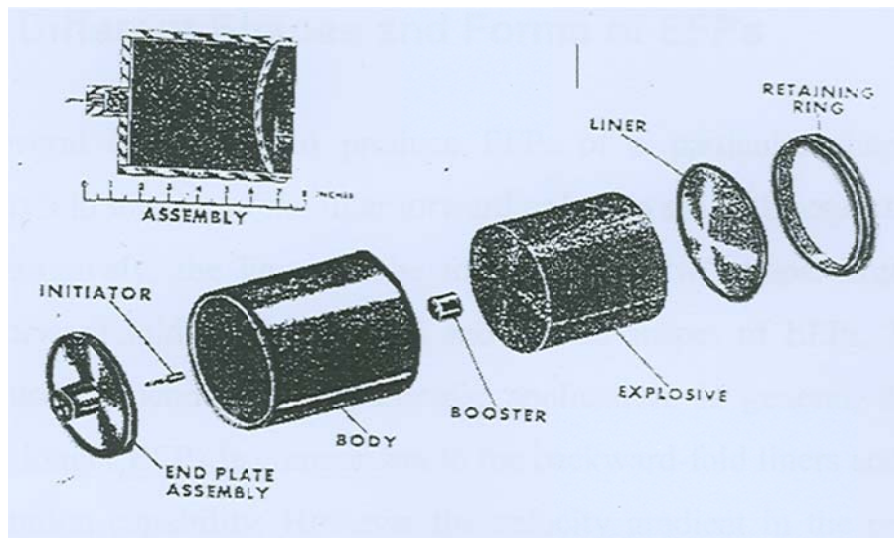


Figure 3.5: components of EFP

Mechanism of explosively formed projectiles (EFPs) is the same as that of shaped charges; hence the liner does not separate into high velocity jet and a low velocity slug. The liner simply folds into a fragment moving off with high velocity. When a detonation wave acts on the liner material, as the liner material is not completely surrounded by explosive, liner is not fragmented, but is expelled by the high pressure gases and is deformed remaining one piece, and moves in the direction of the detonation wave with considerable velocity. In general thinner is the liner the higher is the velocity to which it is accelerated [14].

The self-forging fragment uses the mechanism of explosive forming of a metal liner into a single compact fragment, and projecting it with sufficient velocity to defeat armor at the required extremely long standoffs.

The penetration mechanism is essentially hypervelocity impact. The liner is usually of a curved shape although wide angle conical liners have been considered. The formation of the fragment takes place either by inverting the liner, or by a process basically comparable to shaped charge jet formation but with little or no velocity gradient [18].

3.4 MAJOR COMPONENTS

A typical EFP charge is depicted in Figure 3.5. The device consists of an initiator or detonator a booster and explosive charge encased in charge body with a plate at one end and a hollow metal liner on the other.

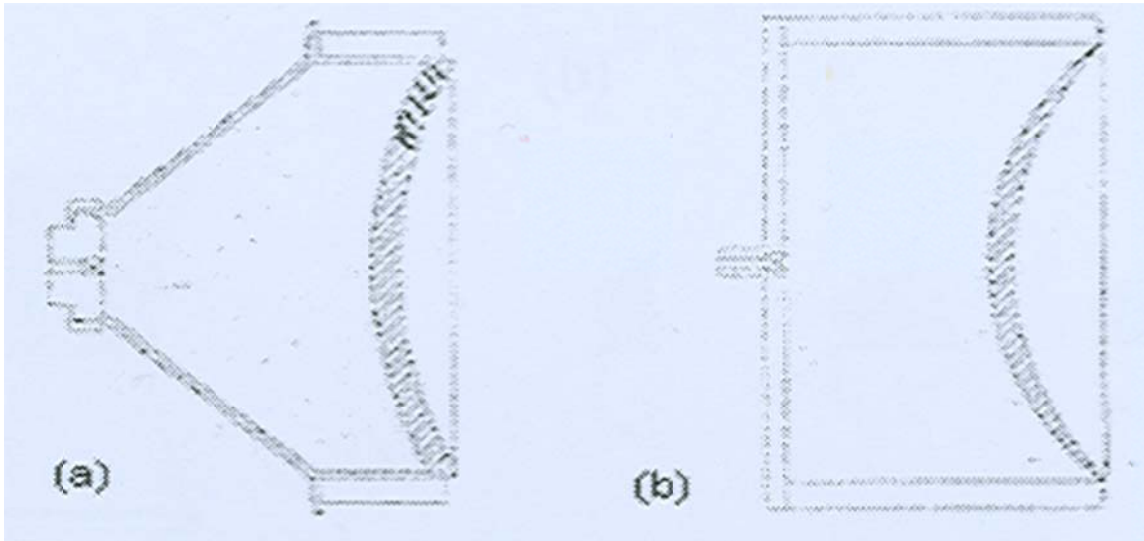


Figure 3.6: Taper casing and cylindrical casing

3.5 DIFFERENT SHAPES AND FORMS OF EFPs

Several techniques can be used to produce EFPs of different final stable shapes. Three types of shapes are prominent (1) forward fold (2) backward fold (3) “w” shaped. Conical liners with uniform thickness gives forward fold shape while contour type thickness gives often backward fold and “w” shaped depending on thickness gradient of the liner. Figure 3.7 shows respectively forward fold; backward fold and w fold shapes of EFPs. Each type of design has its own advantages and applications. Forward fold has longer jet and are used when we need larger penetration in the targets. Forward fold are usually shaped charges with long jet. Backward fold are usually EFPs and are used for larger perforation. It has stable velocity. Ideal for mine’s neutralization. “w” shaped EFPs are used in water application because by passing through water they get solid shape and hence less erosion of mass. [4].

For a particular application a design is chosen. Then its optimization can be done by delicately changing its different parameters. This required experimental test which are very costly and time consuming. Modeling and simulation by using available hydrocodes helps us in this matter. so a combination of experiment and numerical techniques methods

are adopted. Explosive type plays its own roll. HMX gives the largest L/D ratio among all the explosives. Liner thickness types play a very important role in final shape and velocity. [4]

3.6 PARAMETERS AFFECTING THE EFP CHARACTERISTICS

There are several basic parameters in the warhead configuration that affect the projectile shape and performance. These can broadly be classified as geometrical factors and material factors [10]. These factors influence the formation of EFP which include velocity behavior during the flight but also it include affecting its shape, its stability, its velocity and attenuating the velocity profile which is different depending on whether the material is brittle or ductile.

3.6.1 Geometrical Factors

Contours type liners (having variable thickness (thicker in the center as compared with edges)), apex angle of the liners, Explosive charge dimension, confinement configurations, axial thickness and explosive initiation technique are some of the geometrical factors that affect the shape of the EFP [10].

3.6.2 Liner Geometry

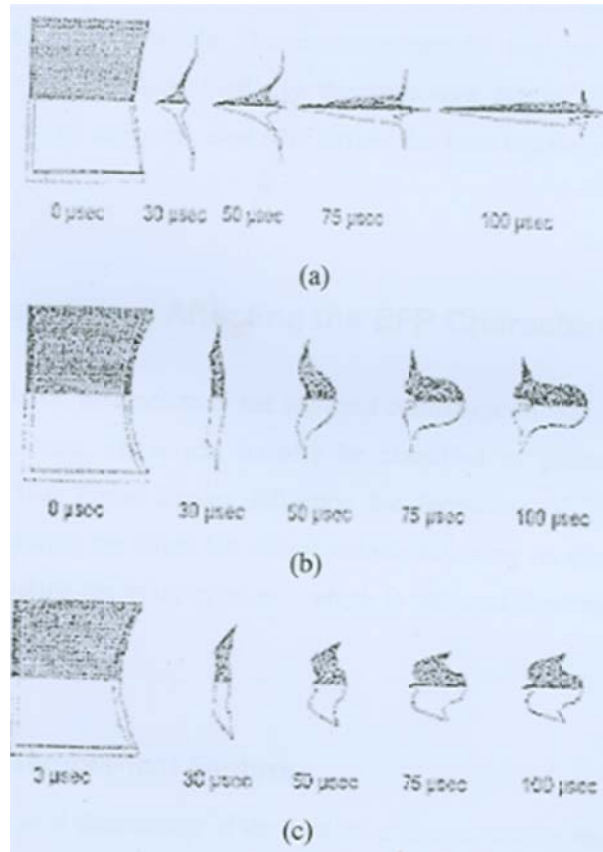


Figure 3.7: Forward, Backward and W Fold EFPs

Weickert and Hallquist found that different liner geometries resulted in forward folding; rear folding or W-fold EFP devices [10]. Shallow dishes are used rather than cones and results can be improved by using a liner with digressive thickness, i.e. dish whose thickness decreases from centre to its edges. This shape encourages the back ward folding of the liner to form a projectile as depicted in figure 3.7. Other liner shapes have also been tried. Ballistic disk liner has w folding, uniform thickness liner has back word folding, and 150° Hyperbolic have forward folding.

3.6.3 Case Confinement

The casing offers a shielding housing (confinement) for the charge and liner, but more important the mass of the casing provides confinement for the explosive. The increasing of mass of the casing increases the duration of the explosive impulse and hence the total energy delivered to the liner [2]. The body may be tapered to create a localized high-pressure effect, called tamping, or it may be uniform, to uniformly increase the detonation pressure or tapered to regulate the velocities of the liner and the confinement.

EFP performance can be improved by changing cylindrical charge to a taper-backed charge and thinning the casing. Mass of charge is also reduced in this case. [4].

Asymmetric casing severely distorted the final shape of the EFP. This effect was studied by Yiu . [2]. If the charge and the liner material were surrounded by a two-piece casing made of 180 of steel and 180 of epoxy. This will be the asymmetric casing. An uneven venting of the explosive products produce distorted shape of EFP. Liner gets unbalanced force. Casing thickness play role in the final shape thicker casing produce solid final shape than thinner casing. In another study [10], it was reported that increasing the casing thickness may break the EFP [10].

3.6.4 Explosive Configurations

The physical dimension of the explosive charge is also of major importance. The length to diameter ratio (LID) is also important. Because of overall system constraints, the explosive charge head height or the length is usually limited. As the charge L/D ratio is increased, the kinetic energy of the EFP increases until to a point of diminishing returns is reached. [2].

3.6.5 Explosive Initiation Technique

Explosive initiation technique also play very important role. Point detonation and line detonation produce different final shape and velocity. Central and off-centre detonation is also very sensitive parameters. Off-center detonation is studied by Johnson

[10] in which the explosive was detonated at a point 1.06 cm above the centerline. Liner gets clockwise rotation initially as it experience shock wave at the upper portion. After some time lower portion gets impulse from the shock wave and the liner stars moving anti-clockwise [10].

3.6.6 Detonation Wave and final shape

Final shape and velocity of the EFP strongly depends on intensity of the detonating wave. The detonating wave will be affected by the

- (i) Explosive type (VOD)
- (ii) Confinement (including quantity)
- (iii) Initiation Technique
- (iv) Geometry of Explosive
- (v) Wave shaping effect

Figure 3.8 shows the predicted effects of typical explosive type on the projectile profile.





		Fragment	
		L/D	Velocity
TNT		0.84	1650 m/s
Comp B		1.65	1950
Octol (75/25)		2.40	2130
HMX		2.65	2160

Figure 3.8: Explosive type and projectile shape

3.7 MATERIAL FACTORS

The material factors include liner material its structure type and its mechanical properties. Similarly casing material and explosive type also included. Processing conditions during manufacturing of liner. [10].

3.7.1 Liner material

The physical and mechanical properties of the liner that are very important are its high density, high melting point, ductility, and these properties are necessary for good dynamic EFP formation process. Copper (cu), tantalum (Ta), iron (Fe) and tungsten (W) exhibit these properties and are the potential candidates for liner material choice. Grain size and hardness of the starting material are also important [10]. The liner material play very important role on the final shape and velocity. Copper liners eroded by passing through water while tungsten made liner show better results.

3.7.2 Casing material

The casing material also plays an important role in the performance of EFP. The casing material should exhibit properties such as high density, high melting point, closed pack crystal structure, good stretch property and no toxicity. The best choice is the steel.it has low cost, high strength and high density. [2].

3.7.3 Explosive material

The important explosive properties are

- (1) Density of the explosive.
- (2) Detonation velocity
- , (3) Explosive energy

Johnson has studied the outcome of a variable density explosive [14] on the EFP formation. As likely, the denser part of the charge imparted a higher velocity to the liner resulting in an angular velocity. Figure 3.8 shows the predicted effects of typical explosive type on the projectile profile [14].

The density of explosive has a significant effect on the symmetry of the formed projectile. If density was higher over one half of the liner relative to the other, it would have much the same effect as the asymmetric confinement described above, with an unbalanced detonation velocity causing the liner to be distorted. Furthermore, if voids were filled in the explosive fill, the liner might be distorted or even torn [2].

3.8 PROCESSING CONDITIONS OF LINER

Faccini and Woodbury studied the reasons for undesirable variance [14] in the performance of Ta EFPs. They investigated the effect of initial annealing, amount of pre strain prior to the initial annealing, amount of Ta removed from the diameter prior to forging, forging temperature, forging rate, liner annealing temperature, and lot using other quality characteristics. They found that different sets of factors affecting different quality characteristics but the material lot, forging temperature and the amount of pre strain were major factors affecting the maximum number of quality characteristics [14]. It is therefore quite apparent that there are many factors that affect the shape and performance of an EFP. EFP efficiency has improved over the years. However things are still to be addressed for the further improvements in the performance of an EFP. [14].

3.9 STANDOFF

The distance travelled by an EFP before it attains stable velocity and shape is called Standoff. Standoff is expressed in charge diameter (CD). It is necessary for an EFP to attain this distance for optimal penetration otherwise there will be less penetration in the target. Optimal penetration (at the appropriate standoff) is usually about one to two charge diameters into steel. Casing and explosive quantity play their role too. At large standoffs, the EFP splits into pieces and hence lesser penetration. [7].

3.10 USES OF EFP

Explosively formed projectiles (EFPs) are related to shape charges but form a fragment rather than a jet. Their long range and high mass and energy make them useful in the following military and civilian applications

- For demolition purposes such as to destroy the building structures and other objects
- Military purposes like linear self-forging anti-armor weapons to defeat the armor at a long standoff in top attack mode.
- To dispose of explosive mines, bombs etc.
- In mining and petroleum industry
- Demolition/Construction Work
- Steel mill furnace tapping
- Glacier blasting, Tree cutting, Hole drilling
- Explosive engraving
- Cutting charges, Safety destruct systems
- To neutralize the sea mines without detonating the explosive encased in them.

3.11 PENETRATION

3.11.1 Mechanisms for defeating armor

When a warhead, such as, kinetic energy (KE) device attack on an armor target, then the behavior of the armor target is calculated by the parameter KE density. At low KE density the target materials respond as solids and the material strength model is responsible for interactions. The most common way of failure is brittle fracture, plastic deformation and plugging. However, for high KE density typically at penetrator velocities in excess of 1000m/s, the resulting stresses are high in comparison to the strength of the target and EFP and therefore behave as fluids.

3.11.2 Long rod warhead penetration

Velocity of the long rod penetration defines its penetration behavior. If it is greater than 1150m/s the hydrodynamic behavior of penetration begins to appear. If less than this plastic deformation behavior. Long rods exhibit both as they have velocities of 1500m/s to 1700m/s.

3.11.3 Shaped charges jet warhead penetration

Shaped charge jet devices have velocities higher than 10,000 m/s, and, therefore, target penetration is always via hydrodynamic flow [24].

3.11.4 EFP warhead Penetration

EFPs and shaped charges are the types of chemical energy devices but they both have different characteristics. Both are used in different applications. EFPs are moderate velocity (1-3km/s) as compared to shaped charges (8-11 km/s). [31]) and evidence has shown that their penetrative performance is much similar to that of long rods [25].

The following equation for hydrodynamic theory can be applied as a an approximation of EFPs

$$P = L\sqrt{\rho_{efp} / \rho_t}$$

Where

P is the Penetration length, L is the Length of EFP, ρ_{efp} is the Density of EFP,

ρ_t is the Density of target material

Gehring and Christman [32] decided that penetration depends upon velocity of EFP and target material strength. The Gehring and Christman give the following relation.

$$P = \left(1 - \frac{D}{L}\right) \left(\frac{\rho_{efp}}{\rho_t}\right)^{\frac{1}{2}} + k \frac{D}{L} \left(\frac{\rho_p}{\rho_t}\right)^{\frac{2}{3}} \left(\rho_p \frac{V^2}{B_t}\right)^{\frac{1}{3}}$$

Where

D is the diameter of EFP, B_t =Brinell hardness of the target material, V is the Velocity of EFP and k is the constant.

The above model allows the final penetration length comes out to be larger than that expected by one dimensional hydrodynamic theory.

Buchholz and Doyle [33] established the following relation.

$$\frac{P}{L} = \left(1 - \frac{D}{L}\right) \left(\frac{\rho_{efp}}{\rho_t}\right)^{\frac{1}{2}} + \frac{0.13}{L} \left(\frac{\rho_{efp}}{\rho_t}\right)^{\frac{1}{3}} \left(\frac{E_t}{B_t}\right)^{\frac{1}{3}}$$

Where

E is the Energy in joules during the last part (caliber) of the EFP.

They say that in the first part behavior is like shaped charge and in the last part behavior is like. Hence the two part equation is established.

EFPs have very much lower velocity than that of shaped charges. EFP penetrative is like long rods penetration. Partial hydrodynamic behavior begins to appear from 1000 m/s and increases regularly. Long rod penetration behavior is described by the Tate and Alekseevkii formula, in which the strengths of the EFP and target material are prominent factors. Experimental evidence has shown EFPs to exhibit long rod penetrator characteristics [34]

The Tate and Alekseevkii equation is

$$\frac{1}{2} \rho_t U^2 + \sigma_t = \frac{1}{2} \rho_{efp} (V - U)^2 + \sigma_{efp}$$

Where

V is the Projectile velocity, U is the Penetration velocity, σ_t is the Target strength,

σ_{efp} is the Penetrator strength

Above Equation suggests that EFP and target material strength play very crucial role in penetration of EFP into the target. However, Tate [29] has shown for $\sigma_t < \sigma_p$ then high velocity both the EFP and target material show hydro-dynamical behavior up to deceleration. When $\sigma_t > \sigma_p$ no penetration. If target strength increases penetration

decreases. This is demonstrated by Weimann et al [30] who has shown that if we increase the target strength from 700 to 1400 MPa reduce penetration by up to 30%. Conversely it would be expected that increases in σ_p increases penetration.

The most features cited in all above penetration equation same. These suggest that for better penetration

- (1) High length to diameter ratio of EFP,
- (2) High density of EFP,
- (3) High velocity of EFP
- (4) High strength of EFP.

3.12 CONCLUSION

The classification of warhead types are presented in this chapter, since our main focus is on the explosively formed projectiles so it is described in detail, including the concept origin, its formation mechanism, its major components and different parameters affecting its performance. The review of regarding material is also given. In the next chapter, the computational aspect of codes developed on the basis of theory related to explosive metal interactions, the set of governing equations involved the computation as well as explosive and liner material properties described in the present chapter, will be outlined. Different problem formulation techniques will also be given.

Chapter 4 System of Governing equations and solution techniques for Explosive Metal Interactions

4.1 INTRODUCTION

The terminal ballistic problems are characterized by intense dynamic loads that are generated by impact or by explosive detonation and that act over time period measured in microseconds. Therefore, inertial effects are dominant in the initial stages, and wave propagation must be adequately simulated.

The general continuum mechanics, used to simulate these phenomena is based upon the conservation or balance equations of mass, momentum, and energy along with response functions describing the behavior of materials. The formulation is completed by specifying initial and boundary conditions appropriate to the problem of interest. The resulting system of partial differential equations is nonlinear and analytic solutions are not usually possible because of the complexity of the initial value problem. Approximate numerical techniques are among the best methods currently available for obtaining complete solutions to these unsteady codes, wave propagation codes, hydrodynamic codes or hydro codes [2].

Hydro codes have emerged as important design tool in the field of warhead engineering. Their use is most effective when integrated directly into the design iteration cycle. For example, the preliminary design of an explosively formed projectile (EFP) can be developed from hydro code calculations that predict the shape and velocity of the projectile. This preliminary design can be built and tested, and flash x ray pictures can reveal the final shape and velocity of the projectile. The test result may differ from the simulation and the desired performance probably will not be achieved by the initial design. At this point the analyst may choose to modify the computational model to obtain better agreement with the test results. Modifications are usually made by adjusting the constants in the material models or by changing the initial setup of the problem [2].

In this chapter, we first review the two types of problems in the impact loading phenomena, the basic principles and associated equation of continuum mechanics that are solved by the hydro codes. Then, a brief review of numerical solution techniques for partial differential equations is presented. The flavor of different problem formulation techniques used in many hydro codes are then given. The hydro code like Autodyn that have been used for warhead simulations is described towards the end of the chapter.

4.2 EXPLOSIVE METAL INTERACTION

The interaction of detonating explosive with a material in contact with it are in close proximity is extremely complex, since it involves detonation waves, shock waves, expanding gases, and their interrelationships. For a simple one dimensional geometry, the sequence of events is qualitatively depicted in figure. 4. 0. A small segment of an infinite explosive slab placed against to a metal plate is imagined in the figure 4.0 (a). The initiation is starting simultaneously over the entire surface of explosive as shown in figure 4.0 (b), producing a pressure pulse that leads to detonation. As the detonation propagates, the greater and greater amount of detonation products accumulating in the left hand side results in a gradual increase of the duration of the pressure pulse, whereas the peak pressure remains constant. This is shown in figure 4.0 (b) & (c). When the detonation front encounters the metal, an interaction will occur and a pressure pulse is transferred to metal depicted in figure 4.0 (d). The peak pressure of this pulse is determined by using the impedance matching technique. Let us assume that $P_2 > P_1$. At the same time, the reflected wave is transmitted into the explosive detonation products. This is shown in figure 4.0 (e). When the shock wave in metal encounters the free surface, it accelerates it at a velocity of $2U_{p1}$ and reflects back a release wave.

This reflected wave will encounter the back face of metal (explosive metal interface) and produce, by interaction, a pressure change figure 4.0 (f). A new shock wave is sent through the metal figure 4.0 (g) that will, in turn, drive the free surface to a velocity that is increased by $2 U_{p2}$. The process continues with successive reflections, $U_{p1} > U_{p2} > U_{p3}$. As the successive reflections take place, the explosive gases continue their

expansion and attenuation of shock wave in the metal takes place. The situation depicted above is one possible sequence. Different wave configuration can occur, depending upon the Chapman Jouquet (CJ) pressure, the metal shock impedance, the thickness of metal and explosive, and the presence of a gap or an attenuator between explosive and metal [17].

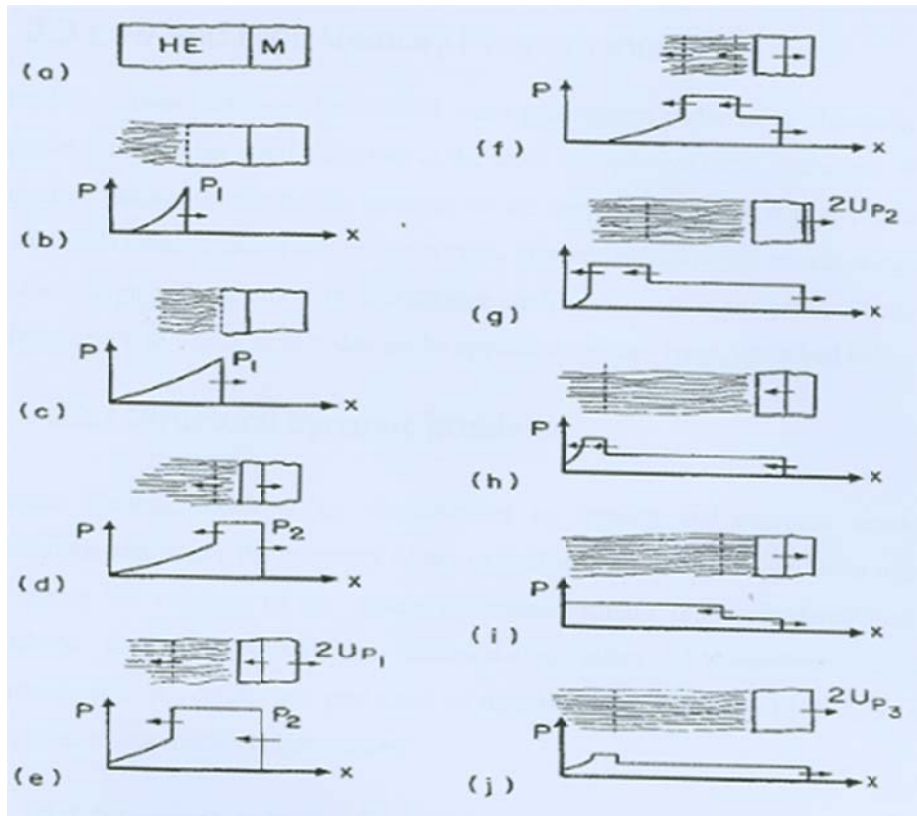


Figure 4.0: pressure-distance plots

4.3 LOW AND HIGH VELOCITY PHENOMENON

A number of two- and three-dimensional wave propagation codes exist. However, the computer codes are not stand alone tool in the study of explosive metal interaction or the penetration phenomenon and their calculations are coupled iteratively with

experiments and material characterization at high strain rates. They are effective tool in achieving cost effective design without excessive computation, testing or material evaluation. Problems or phenomenon to which these codes can be applied are of two types, described below.

4.3.1 Structural dynamic problems

Structure dynamic problems are characterized by loading and response times in milliseconds and where the geometry of the overall structure plays a significant role in determining the response of the system to external stimuli (e.g. safe demolition of pre-stressed concrete structure; the transportation safety of hazardous material; crashworthiness of vehicles and protection of their occupants and cargo) [3]. These are also termed as low velocity phenomenon.

4.3.2 Impact or wave propagation problems

These are characterized by impact or explosive loads where both loadings and response times are in sub millisecond regime Deformation resulting from such loading will be highly localized and determined principally by the constitution and properties of the colliding materials. Representative problem areas include the design of lightweight armor systems, including fabric body armors for protection of police officers and military personnel; protection of spacecraft from meteoroid impact; explosive forming and welding of metals, explosive formation of jets and slugs and jet penetration. These are the high velocity phenomenon [3].

Yet, in both cases there is a common origin since both types can be described mathematically by the wave equation, which in simplest form is

$$c^2 u_{xx} - u_{tt} = f(u_{xx}, u_{tt})$$

Where, u represents a displacement vector, f is a generalized function and subscripts denotes the derivatives with respect to special x or temporal t quantities. In high velocity impact situations, loading and response time are typically measured in nanoseconds to

microseconds. Extremely high pressures are generated that exceeds the several order of the strength of the colliding materials.

4.4 THE GOVERNING EQUATIONS

The equation governing the behavior of solids under impact or impulsive loading conditions are well known, straight forward and can be described in the following section.

4.4.1 Kinematics

Figure 4.1 describes the motion of a body, we refer its configuration to a fixed, three dimensional Cartesian coordinate system. The material particles of the body in its initial configuration (time $t=0$) can be identified by their coordinate values (a_1, a_2, a_3) along 1-, 2-, and 3- axis. At a later time the body move to a new configuration and typical material with initial coordinates (a_1, a_2, a_3) moves to new position with coordinates (x_1, x_2, x_3) . The motion of the body is described by functions that give the current position of its particles in terms of their initial position and time; that is,

$$\begin{aligned}x_1 &= x_1(a_1, a_2, a_3) \\x_2 &= x_2(a_1, a_2, a_3) \\x_3 &= x_3(a_1, a_2, a_3)\end{aligned}\quad 4.1$$

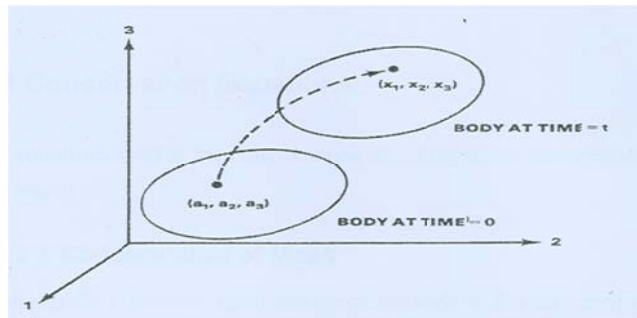


Figure 4.1: Different positions of an object

By using standard indicial notation, these three functions can be written more compactly as

$$x_i = x_i(a_j, t) \quad 4.2$$

Where $i = 1, 2, 3$ and $j = 1, 2, 3$. These mapping functions are numerically determined in Lagrangian hydrocodes calculations. Above equation can be inverted to give the initial position of a particle in terms its current position

$$a_i = a_i(x_j, t) \quad 4.3$$

When the dependent variables of the problem are expressed as function of the independent variable a_1, a_2, a_3 and t , the description is called material or Lagrangian and when the independent variables x_1, x_2, x_3 and t are used, the description is called spatial or Eulerian. The velocity components v_i of a particle (a_1, a_2, a_3) are defined by

$$v_i = \left(\frac{\partial}{\partial t} \right)_a v_i(a_j, t) \quad 4.4$$

Where the partial time derivative is taken with the a_j held constant. The acceleration v_i is defined by

$$v_i = \left(\frac{\partial}{\partial t} \right)_a x_i(a_j, t) \quad 4.5$$

4.4.2 Conservation Equations

Conservation equations used in the computations including mass, momentum and energy are described below.

4.4.2.1 Conservation of Mass

Let $\rho_0(X, t)$ and $\rho(X, t)$ denotes the densities of the body in the reference configuration and current configuration, respectively. The principle of mass conservation may be expressed as

$$\int_{\Omega} \rho_0 dV_0 = \int_{\Omega} \rho dV \quad 4.6$$

Where $dV_0 = dx^1 dx^2 dx^3$ and $dV = J dV_0$ and alternatively, this may be written as

$$\frac{d\rho}{dt} + \rho \frac{\partial v_i}{\partial x_i} = 0 \quad 4.7$$

$\frac{d}{dt}$ Is materials time derivative.

4.4.2.2 Conservation of Momentum

Let σ be the Cauchy stress tensor (referred to and measured with respect to the spatial coordinates X_i), and let f be the body force per unit mass. The local form of the principle of linear momentum is [3]

$$\rho \frac{dv_i}{dt} = \frac{\partial \sigma_{ij}}{\partial x_j} + \rho f_i \quad 4.8$$

4.4.2.3 Conservation of Energy

Let q denotes rate of heat flow per unit area across the surface of body ..., the rate of internal heat generation per unit mass, and T be specific internal energy. Then the local form of the conservation energy may be written as

$$\rho \frac{de}{dt} = \frac{\partial}{\partial x_j} (\sigma_{ji} v_i) - \frac{\partial q_i}{\partial x_i} + \rho s + \rho f_i v_i \quad 4.9$$

The form of conservation equations is similar for Lagrangian (grid fixed in material and distorted with it) and Eulerian (grid fixed in space with material flowing through it) mesh description. The differences occur because of definition of

$$\frac{d}{dt} = \frac{\partial}{\partial t} + v_i \frac{\partial}{\partial x_i} \quad 4.10$$

This derivative known as material derivative, substantial derivative or total time derivative is used in Euler approach in calculating quantities that are transported between cells since they are associated with the mass flow. Thus, conservation equation for an Eulerian system, neglecting heat source and sink, would be [3]

$$\frac{\partial \rho}{\partial t} + \frac{\partial}{\partial x_i} (\rho v_i) = 0 \quad 4.11$$

$$\frac{\partial v_i}{\partial t} + v_j \frac{\partial v_i}{\partial x_j} = f_i + \frac{1}{\rho} \frac{\partial \sigma_{ji}}{\partial x_j} \quad 4.12$$

$$\frac{\partial e}{\partial t} + v_i \frac{\partial e}{\partial x_i} = f_i v_i + \frac{1}{\rho} \frac{\partial}{\partial x_j} (\sigma_{ij} v_i) \quad 4.13$$

4.4.3 Jump Equations

These relationship are derives from the fact that we must conserve mass, momentum and energy across the shock front are called Rankine — Hugoniot Jump equations. [5] These are summaries as

$$\rho_0 U_s = \rho (U_s - u_p) \quad 4.14$$

$$p - p_0 = \rho_0 (U_s - u_p) \quad 4.15$$

$$I - I_0 = \frac{1}{2} (p + p_0) \left[\frac{1}{\rho_0} - \frac{1}{\rho} \right] \quad 4.16$$

Where, ρ (density), P (Pressure), U_s (Shock velocity), u_p (particle velocity) and I is specific internal energy. $v = 1/\rho$, is the specific volume and $v_0 = 1/\rho_0$, The subscript 0 and 1 refer to the state just in front of and just behind the shock front respectively [5].

4.4.4 Constitutive Equations

The conservation laws apply to any continuous material body without regard to its physical constitution. Thus additional relationships that govern both the high pressure (volumetric) and deformation (deviatoric) behavior of body under applied loads are needed. Since impact loading is a very rapid process, we will assume that it is adiabatic (no heat is transferred from the system).

A few additional quantities need to be introduced first. The stress tensor σ_{ij} can be expressed as the sum of hydrodynamic component, $p\delta_{ij}$ and a deviatoric stress, S_{ij}

$$\sigma_{ij} = -p\delta_{ij} + S_{ij} \quad 4.17$$

Where, $S_{ii}=0$: and $\sigma_{ii} = 3p(\rho, I)$

P is obtained from an equation of state. The strain rate tensor and spin tensor are given by

$$\Sigma_{ij} = \frac{1}{2} \left[\frac{\partial v_i}{\partial x_j} + \frac{\partial v_j}{\partial x_i} \right], \quad 4.18$$

$$\omega_{ij} = \frac{1}{2} \left[\frac{\partial v_i}{\partial x_j} - \frac{\partial v_j}{\partial x_i} \right] \quad 4.19$$

The deviatoric strain rate tensor is defined as: [3]

$$d_{ij} = E_{ij} - \frac{1}{3} E_{kk} \delta_{ij}, \dots \dots \dots d_{kk} = 0 \quad 4.20$$

Johnson-Cook Model is used as a strength model in the simulation for Eulerian formulations; it expresses flow stresses in terms of equivalent plastic strain, plastic strain rate and homologous temperature. The yield stress δ is given by equation given below

$$\delta = [A + B \varepsilon^n] [1 + C \ln \dot{\varepsilon}^*] [1 - T_H^m] \quad 4.21$$

The expression in the first bracket gives the stress as a function of strain; expressions in second and third brackets represent the effect of strain rate and temperature respectively.

Where ε^n is the effective plastic strain and dimensionless $\dot{\varepsilon}^*$ strain rate. A is yield stress constant, B is strain hardening coefficient, n is strain hardening exponent, C is strain rate dependence coefficient and m is temperature dependence exponent. T_H is homologous temperature and is given by equation given below

$$T_H = (T - T_{ref}) / (T_{melt} - T_{ref}) \quad 4.22$$

Heat is generated in an element by plastic work and the resulting rise in temperature is computed using specific heat for the material.

Zerilli-Armstrong constitutive equation can also be used as a strength model in the simulation for Eulerian or Lagrangian formulations. The yield stress σ is given by following equations for both face centered cubic (FCC) and body centered cubic (BCC) crystals:

Zerilli-Armstrong (FCC)

$$\sigma = \sigma_0 + C_2 \Sigma^{1/2} \exp[-C_3 T + C_4 T \log \Sigma] \quad 4.23$$

Zerilli-Armstrong (BCC)

$$\sigma = \sigma_0 + C_1 \exp[-C_3 T + C_4 T \log \Sigma] + C_5 \Sigma^n \quad 4.24$$

Where C_1, C_2, C_3, C_4 and C_5 are the hardening constants number 1, 2, 3, 4 and 5 respectively, Σ is the effective plastic strain and n is strain hardening exponent.

4.5 NUMERICAL METHODS AND SOLUTION TECHNIQUES

A computer program that uses finite difference, finite volume or finite element techniques to solve non-linear problems is often referred to as a “hydrocode” [8]. The method most commonly employed by hydrocodes is the method of finite differences. In its simplest form, derivatives occurring in the differential equations are replaced by difference approximations. This replacement produces a system of algebraic equations that can be solved for the dependent variables at the node points, or lattice points of a finite difference mesh [2].

The phenomena to be studied with such a program, in the scope of this literature review, can be characterized as highly time dependent with large strains and stresses (geometric non-linearity) and plasticity, failure, hardening and softening, and multiphase equation of state (material non-linearity) [7].

A key interest in developing advanced simulation tools (computer codes and material models) is to examine a range of parameter variation of a protection configuration (materials, spacing, layers and threat) [9], even at impact velocities too great for experimental studies. Analysis and simulation with hypervelocity impacts are required for space vehicles [7].

Simulation of explosive loading phenomenon and high velocity penetration is based on a continuum mechanics formulation using the equation of mass, momentum and energy conservation, together with appropriate description of material behavior. The formulation is completed by specifying initial boundary conditions appropriate to the problem of interest. The resulting system of partial differential equations is non-linear; hence the need for numerical evaluation is needed in situations where simplifications are not appropriate. The problems addressed by such computations involve intense dynamic loads generated by impact or explosive detonation acting over extremely short time periods (nanoseconds to microseconds). Inertial effects dominate initial stages and the interaction of stress wave with material boundaries, geometric boundaries and each other must be adequately simulated [3].

4.5.1 Important Concepts in Numerical Simulations

There are a few expressions that often occur in connection to numerical simulations. Short descriptions of some of these expressions are given in the following section.

4.5.1.1 The Finite Element Method

The finite element method is a numerical procedure for analyzing structures and continua [34], which originated as a method of stress analysis. Today it is also used to analyze problems of heat transfer, fluid flow, electric and magnetic fields and many more. A definition of the finite element method may be [9]: “a method of piecewise approximation in which the approximating function is formed by connecting simple functions ϕ , each defined over a small region (element). A finite element is a region in Space in which a function ϕ is interpolated from nodal values of ϕ on boundary of the Region in such a way that inter element continuity of ϕ tends to be maintained in the Assemblage”.

The power of the finite element method is its versatility. The method can be applied to various physical problems and it has a close physical resemblance between the actual structure and its finite element model. The numerical methods also have disadvantages. A specific numerical result is found for a specific problem: it provides no closed-form solution that permits analytical study of the effects of changing parameters. Experience and good engineering judgments are needed in order to define a good model; the extensive documentation of a general purpose program cannot be ignored. Depending on the unknowns and dependent variables the method can be qualified with words like displacement, force and hybrid or mixed [7].

4.5.1.2 The Finite Difference Method

The finite difference method is a method in which a numerical solution of the differential equation for displacement or stress resultant is obtained for chosen points on the

structure, referred to as nodes or pivotal points. The numerical solution is then obtained from differential equations which are applicable to the actual continuous structure. This is different from the finite-element method, in which the actual continuous structure is idealized into an assembly of discrete elements. The numerical solution by finite differences generally requires replacing the derivatives of a function by difference expressions of the function at the nodes. The differential equation governing the displacement (or stress) is applied in a difference form at each node, relating the displacement at the given node and nodes in its vicinity to the external applied load. The finite-difference coefficients of the equations applied at nodes on, or close to, the boundary have to be modified compared to the coefficients used at interior points, in order to satisfy the boundary conditions. Therein lies one of the difficulties of the method and a disadvantage in its use compared with the finite element method [7].

4.5.1.3 The Finite Volume Method

This is a numerical model for solving partial differential equations that calculates the values of the conserved variables averaged across the volume. It does not require a structured mesh which is an advantage over the finite difference method. The values of the conserved variables are located within the volume element, not at the surfaces or nodes. This makes it possible that boundary conditions can be applied non-invasively [12]. These kinds of methods are powerful in calculations where the mesh moves to track interfaces of shocks [7].

4.5.2 Problem Formulation Techniques

A formulation technique must be chosen when a problem is defined in a hydrocode if the code allows more than one technique. Many codes allow the user to use different techniques in different parts of the problem definition.

4.5.2.1 Lagrangian formulation

A Lagrangian coordinate system, in which the coordinates move with the material, is suitable for following the flow in regions of relatively low distortions and possibly large deformations.

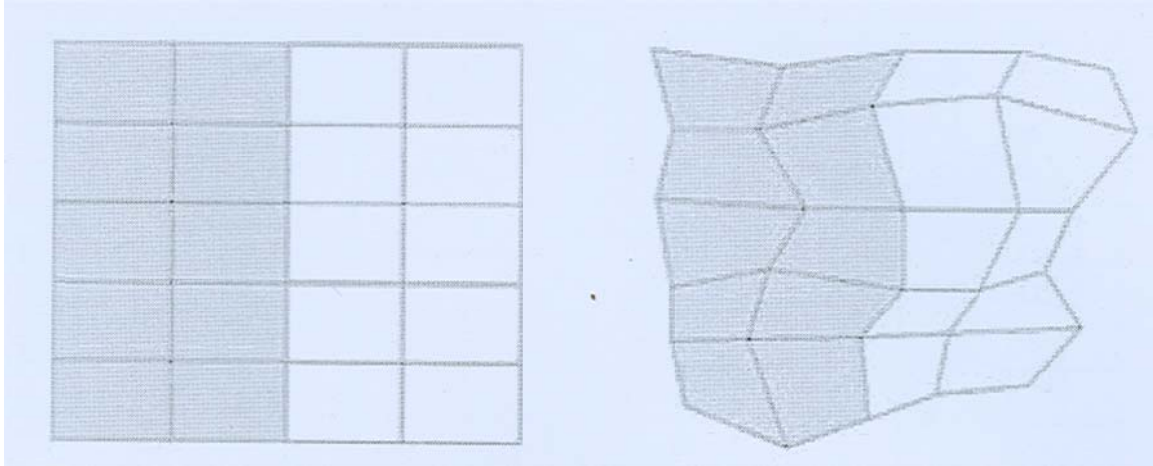


Figure 4.2: Lagrange mesh deformation

The Lagrangian coordinate system will deform with the material and therefore accurately define material interfaces, as shown in figure 2.3. The history of the state of the material in a cell is known completely. Compared to the Eulerian method the Lagrange method tends to be faster computationally as no transport of material through the mesh needs to be calculated. Material interfaces, free surfaces are generally easier to follow with Lagrange formulation than with an Eulerian formulation. A major drawback of the Lagrangian formulation is that if excessive material movement occurs, the numerical mesh may become highly distorted leading to an inaccurate and inefficient solution. The numerical mesh can be remapped to a more regular mesh to reduce the mesh distortion problem. Other techniques such as (numerical) erosion can also be used [8].

4.5.2.2 Eulerian formulation

In Eulerian codes the material flows through the mesh as depicted in figure 2.4. This is often done in two steps or phases. In the first step (Lagrangian phase), the mesh is allowed to deform as the problem is advanced in time and then, in the second step (advection phase), the distorted mesh is remapped back to the original mesh. The material interfaces are not well defined in Eulerian codes, as seen in Figure 8, due to the material flow through the mesh. The interface between two dissimilar materials is known at best to within some fraction of a cell dimension. These interface cells contain materials of both the bodies involved in contact and therefore are designated as “mixed cells”.

Today most Eulerian hydrocodes use a material interface reconstruction scheme. Even with a perfect material reconstruction algorithm, problems may occur when two material boundaries of the same material come in contact. In this case the interface can simply disappear, and the materials behave as one material [1 1].

4.5.2.3 Advantages and disadvantages of Lagrange and Euler formulation

A summary of advantages and disadvantages with Lagrangian and Eulerian formulations is given. Advantages of Lagrange: (1) Material boundaries and interfaces are clearly defined and do not mix. (2) information of load history (3) sharper mapping of shock waves. (4) simple program code (5) shorter calculation time. Disadvantages of Lagrange (1) severe element cell distortion and hence longer calculation time. (2) cell distortion may cause the simulation to stop and program to abort.

Advantages of Euler: (1) no grid distortion and stopping of simulation. (2) larger deformation possible (3) possibility of material mixture. (4) flow calculation possible. (5) requires more calculation time. Disadvantages. (1) needs finer mesh. (2) less adequate description of strength variation in time.

4.5.2.4 ALE (Arbitrary Lagrangian-Euler)

The ALE method is an extension of the Lagrangian method that, via additional computational steps, moves the grid and remaps the solution onto a new grid [1 1]. One

promise of this technique is that the freedom in dynamically defining the mesh configuration should allow a combination of the best features of both Lagrange and Euler [7].

4.5.2.5 SPH (Smooth Particle Hydrodynamics) formulation

The SPH technique uses no grid; it is a pure Lagrangian particle method. (Libersky 1993) The absence of a mesh and the calculation of interactions among particles based on their separation alone means that large deformations can be computed.

A foundation of the SPH technique is interpolation theory. The conservation laws are transformed from partial differential equations into integral equations through the use of an interpolation function that gives the “kernel estimate” of the field variables at a point. (Libersky 1993) The reason why an underlying grid is not needed is that functions are evaluated using their values at the discrete points (particles) and an interpolation kernel [7]. Following figure 2.5 shows the Undeformed (left) and deformed (right) bodies in SPH formulation.

4.5.2.6 Molecular Dynamics

Despite differences in computer realization, both Lagrangian and Eulerian techniques concern the same physical model based on the Navier-Stokes equations (Dzwiniel 1996). The principal assumptions of this model are: mass, momentum and energy flow continuity and thermodynamic equilibrium in differential volume. These assumptions fail for at least two important cases:

1. Investigations of microscopic mechanical properties of materials.
2. When the material considered is brittle, porous and the kinetic energy of the projectile is transferred mainly into mechanical energy of the target not changing the material properties.

These problems can be reduced by using the molecular dynamics approach. In the micro scale the material has to be seen as an ensemble of separate particles. In this scale the assumptions concerning matter, momentum and energy flow continuity and

Thermodynamic equilibrium in differential volumes are no longer valid (Dzwiniel 1996). Instead of Navier-Stokes based models, molecular dynamics have to be used. The Principles and assumptions of one (Dzwiniel 1996) computational model with molecular Dynamics (MD) can be summarized as:

1. Both target and projectile are composed of particles.
2. Particles interact via short range potential.
3. Particle moves according to the Newtonian laws.
4. The model is two-dimensional.

With MD it is possible to simulate discontinuities like cracks and fragmentation of Matter, in a way that is not allowed by continuous hydrocodes (Dzwiniel, 1996) [7].

4.5.3 Equation of State (EOS)

Hydrocodes utilize differential equations for material dynamic motion to express the local conservation of mass, momentum and energy. To be able to obtain a complete solution, also considering initial boundary conditions, it is necessary to define a further relation between the flow variables. This can be found from a material model which relates stress to deformation and internal energy. It is, in most cases, possible to separate the stress tensor into a uniform hydrostatic pressure and a stress deviatoric tensor associated with the resistance of the material to shear distortion. This relation between the hydrostatic pressure, the local density (or specific volume) and local specific energy (or temperature) is known as an equation of state (EOS) [8].

The equation of state for a metal is based on two parts the hydrostat, which describe the volumetric variation with pressure and energy, and the constitutive relations, which describes the stress strain behavior of the material. It must be realized, however, that strictly the Mie-Gruneisen equation of state only applies to states close to the reference curve, because of the definition of the Gruneisen Gamma.

In thermodynamics texts, equation of state means a relationship between P , v and T , such as $P V = RT$ or a more complicated relationship such as the Van der Waals equation of state. In the field of shock wave physics, the equation of state seems to mean whatever

information about the material properties will allow the user to proceed to a solution of the problem that is of interest at the moment [4]. Following are different equation of states:

4.5.3.1 Ideal Gas equation of states

The simplest equation of state to start with is ideal gas equation of state is the relation between pressure volume temperature and universal gas constant R [5].

$$PV = RT \quad 4.24$$

4.5.3.2 Noble Able equation of states

It is simple modification in the ideal gas equation of state, where v is the co-volume and b is constant.

$$P(v - b) = RT \quad 4.25$$

4.5.3.3 Tait Equation of State

The Tait equation of state is of the form

$$E - E_0 = \frac{(p+a)v}{\Gamma_0} - \frac{(p_0+a)v_0}{\Gamma_0} \quad 4.26$$

Where a, is the pressure constant, p is pressure and v the specific volume and Γ_0 is Gruneisen gamma. Tait equation of state is useful for treating solids and liquids, because it allows the sound velocity to be chosen to fit the experimental value at zero pressure [4].

4.5.3.4 BKW Equation of State

The Becker-Kistiakowsky-Wilson (BKW) equation of state has been calibrated for estimating detonation properties. It has the form:

$$\frac{PV}{RT} = 1 + \frac{b}{v(T + \theta)^a} \exp \left[\frac{\beta b}{v(T + \theta)^a} \right] \quad 4.27$$

Where, B and b are constants, & is temperature constant in BKW equation of state, a is exponent in BKW equation of state, p is pressure, v the specific volume and T be the temperature [4].

4.5.3.5 JWL Equation of State

For design of devices using high explosive, simple equation of state that can be easily recalibrated are needed [4].

The equation of state most commonly used to describe the behavior of the detonation products of explosives in applications of metal acceleration is the Jones-Wilkins-Lee (JWL) equation given by

$$p = A_{jwl} \left[1 - \frac{\omega}{R_1 V} \right] e^{-R_1 V} + B_{jwl} \left[1 - \frac{\omega}{R_2 V} \right] e^{-R_2 V} + \frac{\omega}{V} E \quad 4.28$$

In this equation A_{jwl} , B_{jwl} , R_1 and ω are constants for particular explosive, V is the relative volume (volume of products/volume of undetonated high explosive HE) and E is the relative internal energy(energy/volume of undetonated high explosive HE) [2].

4.5.3.6 Mie Gruneisen Equation of State

The equation of state for inert solids is the Mie Gruneisen given by:

$$p = p_H + \rho \Gamma (e - e_H) \quad 4.29$$

In the above equation F and e & e functions of density only, represent the pressure and internal energy on the principle Hugoniot curve, and Γ is Gruneisen parameter (gamma) defined by

$$\Gamma = \frac{1}{\rho} \left[\frac{\partial p}{\partial e} \right]_e \quad 4.30$$

An EOS can be expressed either by an analytic equation (or several equations), or by a table of numbers. Parameters for the Mie Gruneisen Equation of State are summarized in table 2.6.

Much work has been done to describe models for different materials, since each material requires its own EOS. The more complex the material is, the more complex the model will become. There may be a need of a set of EOSs if the material may undergo phase changes during the simulation.

- 1 . Shock response
2. Material compaction (particularly in Nextel which is macroscopically porous)
- 3 . Phase changes (particularly epoxy vaporization)
4. Material anisotropy
5. Anisotropic strength degradation
6. Coupling of volumetric and deviatoric response.

The anisotropy, porosity and complex failure mechanisms could be neglected if the material being modeled is aluminum [7].

The only practical way of obtaining data on the behavior of the material at high strain rates is to carry out well-characterized dynamic experiments [8].

4.5.4 Hydrocodes

A short description of some of the hydrocodes that are used for simulations of behind armour debris will be given below.

4.5.4.1 AUTODYN

The AUTODYN programs are general-purpose engineering software packages that use finite difference, finite volume and finite element techniques to solve non linear problems in solid, gas and fluid dynamics [32 means 8]. AUTODYN are released in both 2D (from 1986) and 3D versions (from 1991). AUTODYN employs a coupled methodology to allow a numerical solution for a given problem. Different domains of a physical problem can be modeled with different numerical techniques most appropriate for that domain. The code then couples these domains together in time and space to provide a solution. AUTODYN includes the following numerical processors [8]:

1. Lagrange processor for modeling solid continua and structures.

2. Euler processor for modeling fluids, gases and large distortions.
3. ALE (Arbitrary Lagrange Euler) processor for specialized flow models.
4. Shell processor for thin structural elements
5. SPH (Smooth Particle Hydrodynamics)

All the numerical processors use explicit time integration. Libraries of material data are included. AUTODYN is a product marketed by Century Dynamics [7].

4.6 CONCLUSION

In this chapter, we presented the two types of the impact loading phenomena, the basic principles and associated equations of continuum mechanics that are used by the Hydrocodes. Then, a brief review of numerical solution techniques for partial differential equations is presented. The flavor of different problem formulation techniques used in many hydrocodes and Autodyn used for warhead simulations are given. In the proceeding chapter numerical techniques adopted for EFP simulations will be described.

Chapter 5 Results and Discussion

Numerical simulations can be used to extract the material response in pressure and temperature regimes beyond the available experimental and diagnostic capabilities. Numerical studies require less time and can be performed at lower cost than experimental studies. Effect of small changes in numerical simulation of a problem design require less effort as compared to experimental configuration which may require additional machining and assembling of hardware and are time consuming .[18]

5.1 DESIGN 1 [25]

The liner material is made up of commercially available high conductivity copper. Liner thickness is uniform (4mm).charge diameter is 60mm.Liner diameter is also 60mm. Casing is 3mm Aluminum. Length to diameter (L/D) is equal to 1.16. Target is 1006 steel 65mm. and it is hit when projectile gets stable shape and velocity. Point detonation at (4, 0) co-ordinates is applied.

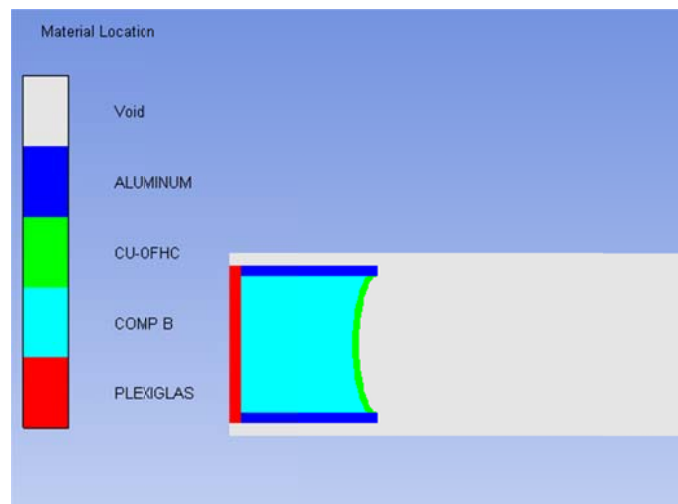


Figure 5.1: Initial stage of design 1

Table 5.1: Design parts and their EOS and Material Models,

Component	EOS	Material Model
CU-OFHC	Shock	Steinberg Guinan
COMB B	JWL	NONE
STEEL 1006	Shock	Johnson Cook
WATER	Shock	NONE
PLEXIGLAS	Shock	NONE

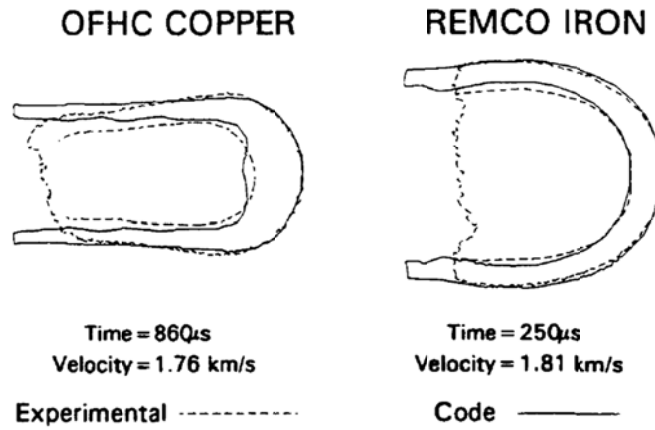


Figure 5.2: Reference results and final shapes of EFPs [25]

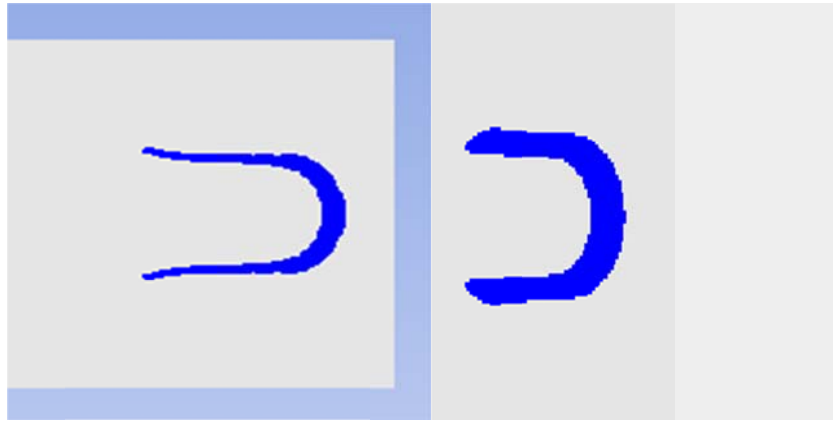


Figure 5.3: Simulation results for copper and Iron at reference times.

Table 5.2: Comparison of Experimental and Simulation Results for Design 1

	Experiment	Simulation	% Diff	Liner
Velocity(km/s)	1.76	1.702	3.30	Cu-OFHC
L/D	1.5	1.39	7.00	
Velocity(km/s)	1.81	1.82	0.55	Armco Iron
L/D	1.0	1.03	3.00	

5.1.1 Conclusion:

Stable velocity, shape and L/D ratio matches with experimental[25] results .For Cu-OFHC the stable Velocity at time 860 μ sec is 1.702 km/s and experimental was 1.76km/s. For Armco Iron the stable Velocity at time 250 μ sec is 1.82 km/s and experimental was 1.81km/s.



Figure 5.4: Comparison of target penetration cross-section produced by Fe EFP.

5.1.2 Conclusion:

Simulation results are in good agreement with experimental results for Iron.

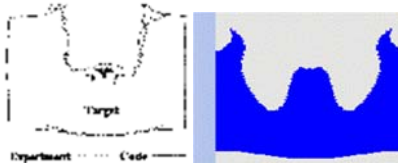


Figure 5.5: Comparison of target penetration cross-section produced by Cu EFP.

5.1.3 Conclusion

Simulation results are in good agreement with experimental results for Cu EFP.

5.2 DESIGN 2

Liner material is made up of commercially available high conductivity copper. Casing is 3mm 1006 steel. Explosive head height is 30mm. charge diameter is 60mm

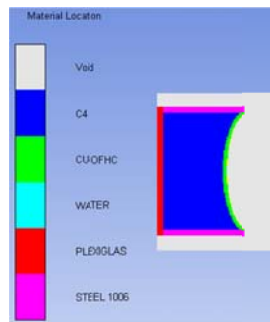


Figure 5.6 Initial stage of design 2

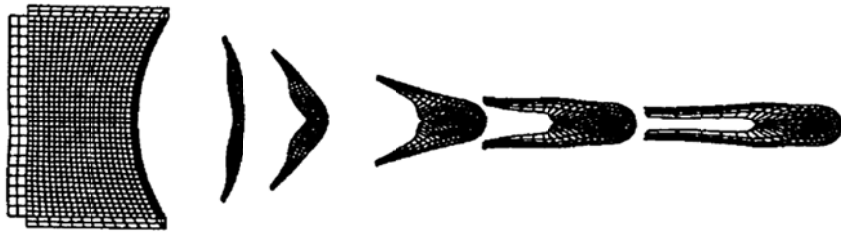


Figure 5.7 Simulation done by C. Lam at time 0 20 30 50 70 and 100 μsec [24]

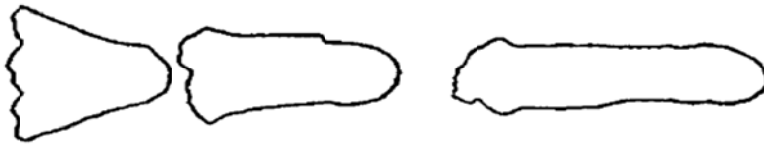


Figure 5.8 Experiments taken snapshots at time 50, 70, 100 μsec [24]

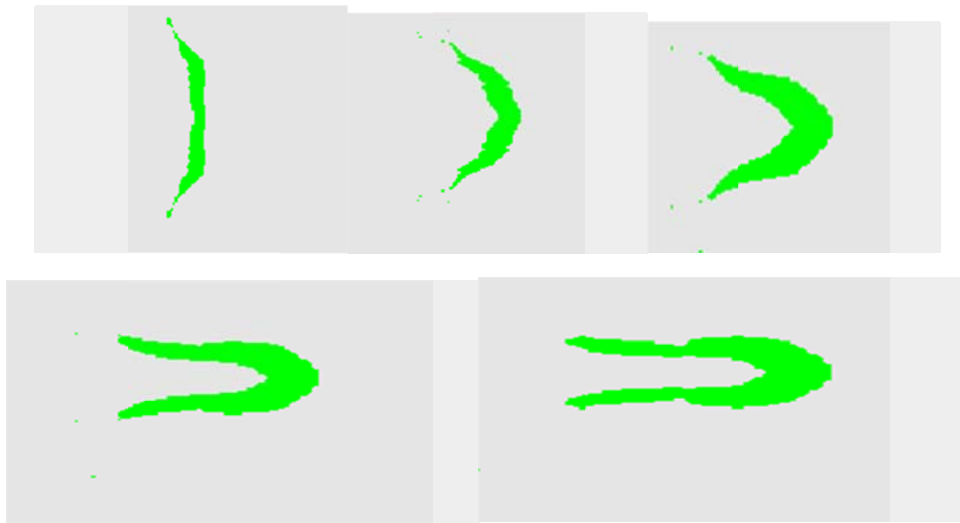


Figure 5.9: simulation done at time 20 30 50 70 and 100 μsec

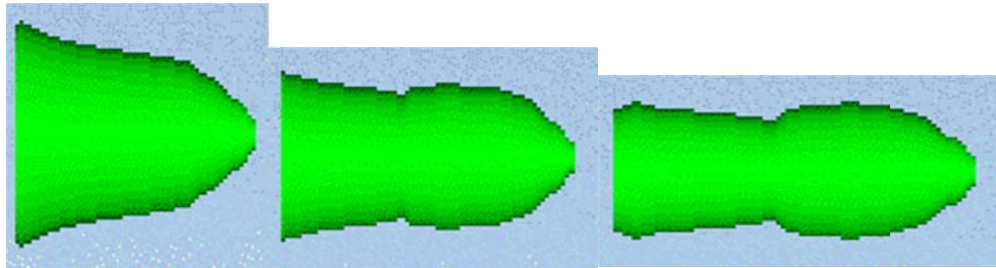


Figure 5.10: simulation done at time 20 30 50 70 and 100 μsec (3d view)
 As it is seen from figure 5.10 and 5,8 the shapes well matches at times 50,70 and 100 μsec . stable velocity as noted by simulation is 2.1km.s and experimental was 2.0km/s.

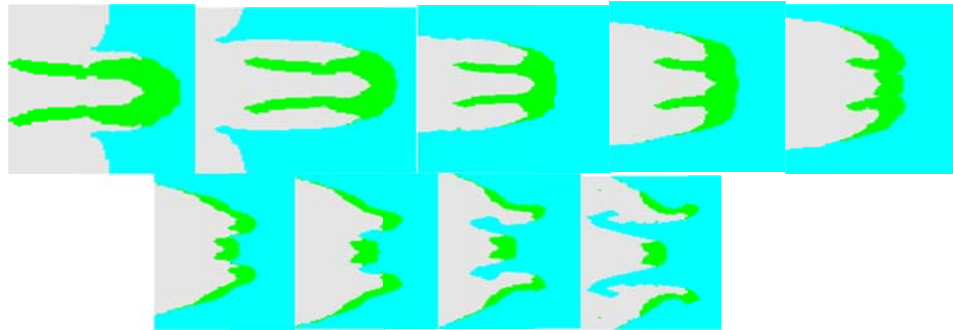


Figure 5.11: Elongated EFP passing through water at times 110, 120, 140, 150,160, 180,190, 210 and 230 μsec



Figure 5.12 Experiments taken snapshots at time 120, 150 μsec [24]

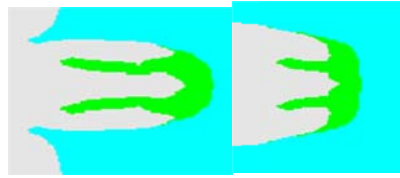


Figure 5.13: Elongated EFP passing through water simulation results at times 120 150 μsec [24]

Shape well matches with experimental results. Liner breaks after 180 μsec and unable to get its task. so elongated EFPs are not recommended for water penetration in case of copper made liners EFPs. Fig 5.14 shows the rapid decrease in velocity while passing through water .it covers only 2.5CD distance in water and its velocity decreases from 2 to 0.55km/s. so we have to switch over to another design or material.

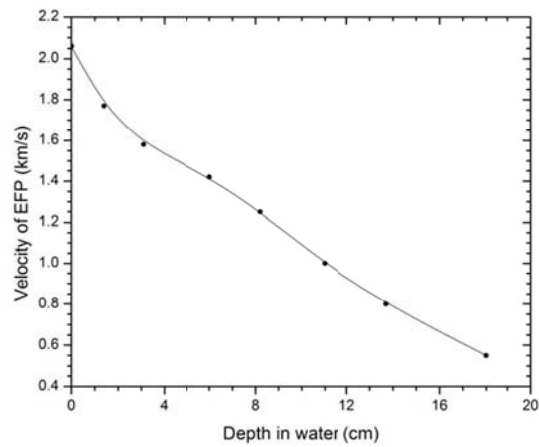


Figure 5.14: Elongated EFP passing through water

Table 5.3: Design parts and their EOS and Material Models,

Component	EOS	Material Model
CU-OFHC	Shock	Steinberg Guinan
C4	JWL	NONE
STEEL 1006	Shock	Johnson Cook
WATER	Shock	NONE
PLEXIGLAS	Shock	NONE

5.3 DESIGN 3

Initial configuration of the design 3-A is shown in the figure below

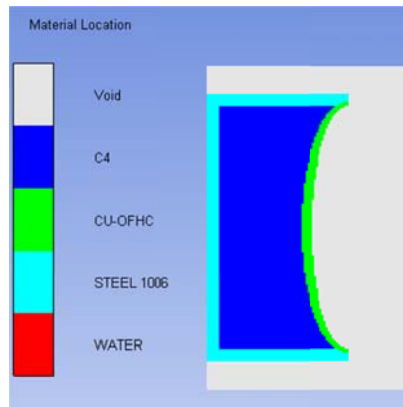


Figure 5.14: Initial Design 3

The liner material is made up of commercially available high conductivity copper. Liner thickness is contour type (central thickness is 3mm outer most is 2mm) having diameter is 60 mm. Casing 3mm Aluminum. Explosive head height is 30% of the charge diameter. The water column is 100 mm away from the initial position of the liner.

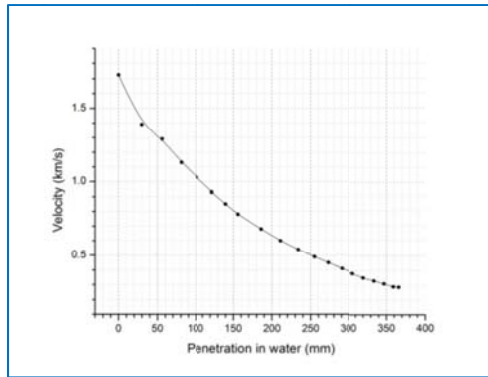


Figure 5.16: Velocity profile of EFP in water design 3

5.3.1 Conclusion:

Better penetration and less erosion of mass of EFP.

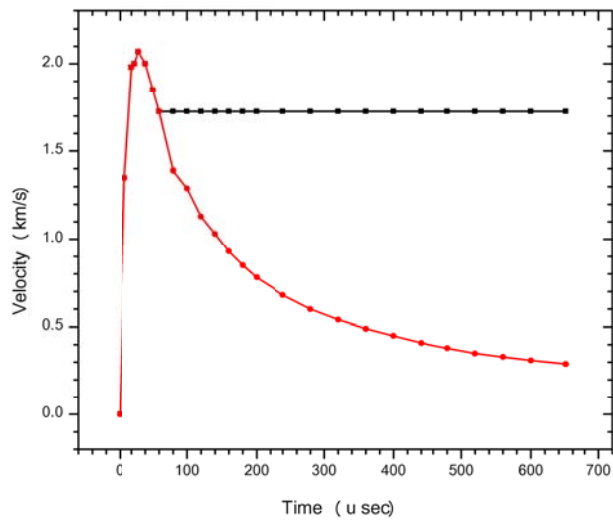


Figure 5.17: Velocity profile of EFP in void water design 3

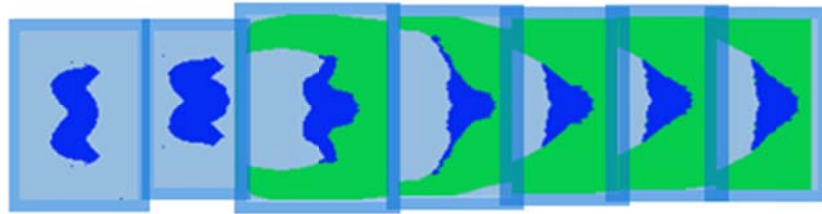


Figure 5.17a: W-shaped EFP on the way in void and water at 40, 60, 80,100,200,400,662 μsec

The w-shaped EFP has got solid shape by passing through water. It does not break as in the case of elongated EFP. Better penetration than that of previous design. Its stable velocity in void is 1.72km/s. it covers 4.0D distance in water as its velocity decreases from 1.72 to 0.55km/s.

5.4 DESIGN 4 (DUMPLING)

The liner material is made up of commercially available high conductivity copper. Liner thickness is contour type (central thickness is 3.8mm outer most is 2.5mm) having diameter is 60 mm. Casing 3mm 1006 steel. Explosive head height is 33.34% of the charge diameter. The water column is 235 mm away from the initial position of the liner.

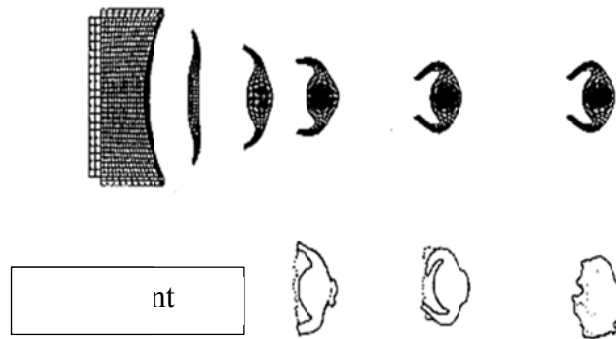


Figure 5.18: dumpling EFP at times 60, 90 and 150 μsec [24]

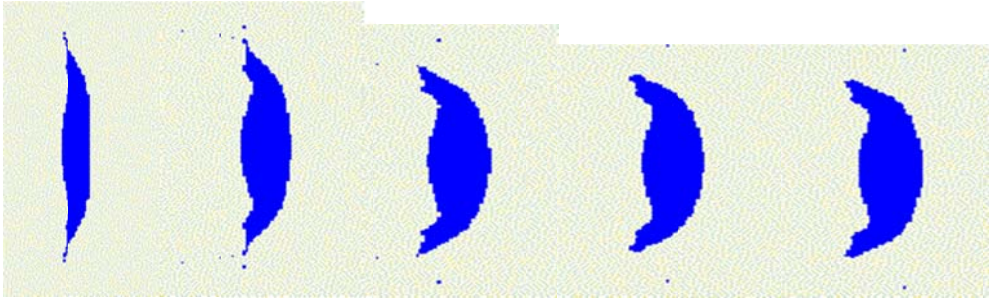


Figure 5.19: dumpling EFP shape profile at times 20, 40, 60, 90 and 150 us

Conclusion: (1) velocity of stable EFP from simulation is 1.48 and from experiment is 1.44. So % difference is 2.77% (2) Shape is very much similar (3) Penetration profile in water is shown in figure 5.20 below . it covers 2.5.0D distance in water as its velocity decreases from 1.48 to 0.55km/s.

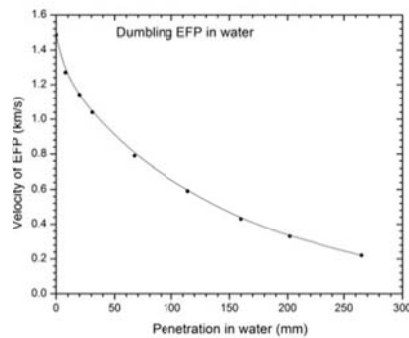


Figure 5.20: dumpling EFP through water

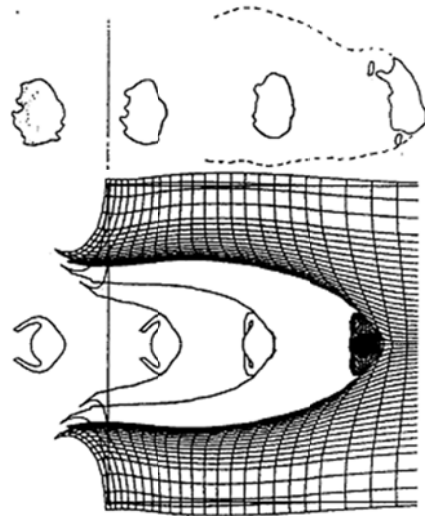


Figure 5.21: dumpling EFP [24]

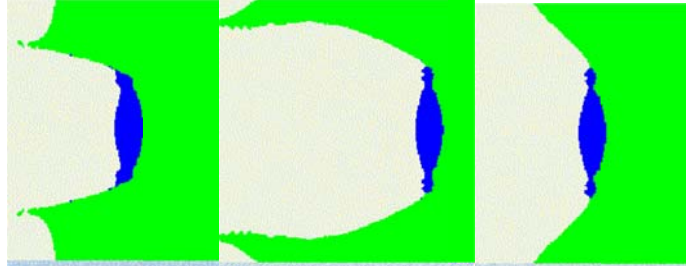


Figure 5.22: shapes of dumpling EFP in water

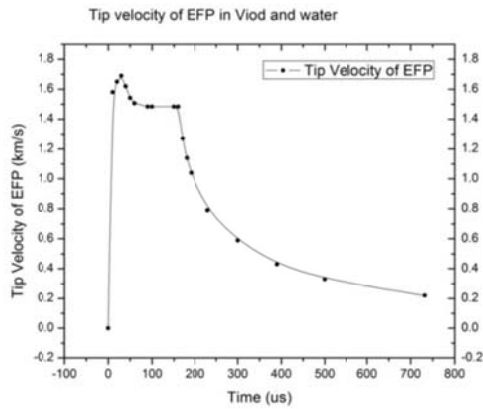


Figure 5.23: dumping EFP Velocity profile in void and in water

5.5 DESIGN 5 (FINAL HEART SHAPE)

The liner material is made up of commercially available high conductivity copper. Liner thickness is contour type (central thickness is 3.5mm outer most is 0.5mm) having diameter is 60 mm. Casing 3mm 1006 steel. Explosive head height is 33.34% of the charge diameter. The water column starts from 180mm of the grid.

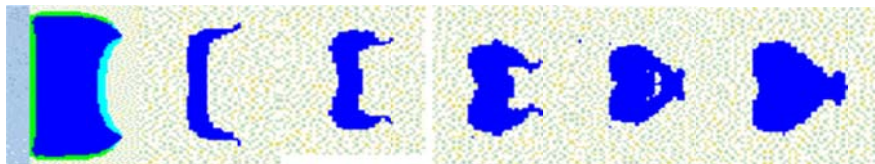
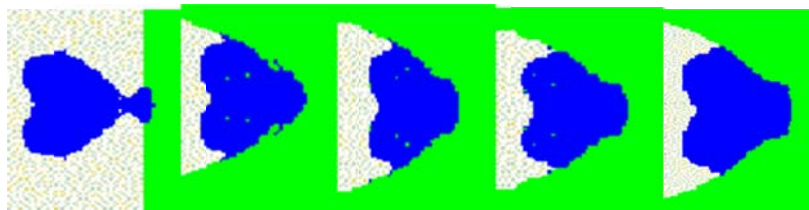


Figure 5.24: Heart EFP formation steps at 10 20 30 40 50 and 60 μsec

Formation steps of EFP in void at 10 20 30 40 50 and 60 μsec. its stable velocity is 1.63km/s. it has good final solid shape.



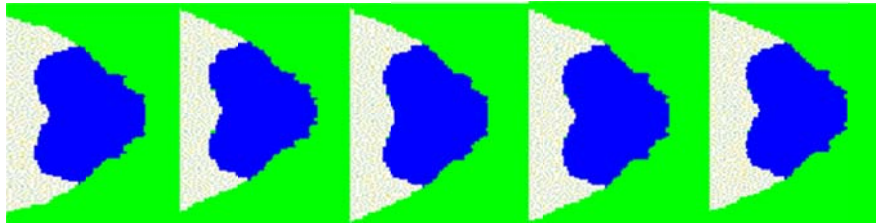


Figure 5.25: Heart EFP penetration in water at 90, 110, 120, 130, 185, 310, 660, 1010
1360 and 1610 μsec

Heart type EFP has very less erosion due to solid shape and hence much better penetration, as compared to uniform liner thickness contour type and W-shaped EFPs. It covers 8.3.CD distance in water as its velocity decreases from 1.63 to 0.55km/s as seen from figure 5.27.

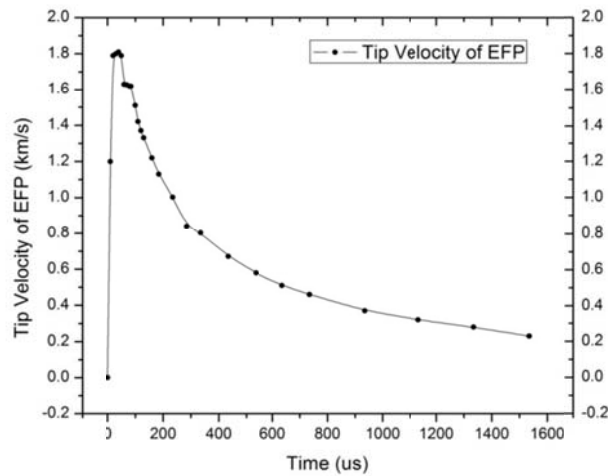


Figure 5.26: Heart EFP Velocity profile in void and in water

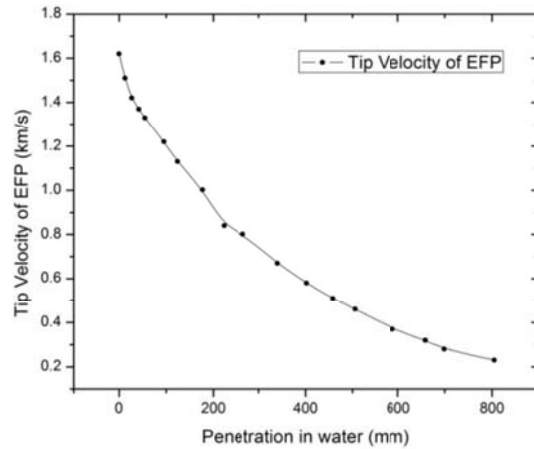


Figure 5.27: Heart EFP Velocity profile in water

5.6 DESIGN 6

The liner material is made up of Tungsten. Uniform Liner thickness is equal to 2mm having diameter is 60 mm. Casing 6mm 4340steel. Explosive head height is 60mm. L/D ration (60/60=1.0). The water column starts from 240mm and ends at 1000 mm. Here we have taken five cases of this design to see the effect of linear curvature on the final parameters.

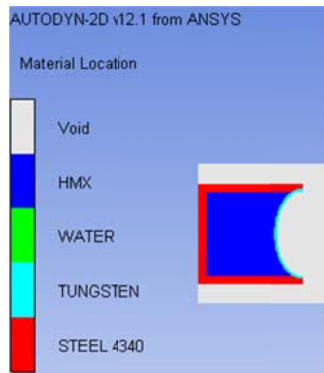


Figure 5.28: formation of Tungsten EFP in void

- Theta or apex angle 139 degree
- Theta or apex angle 133 degree (better penetration)
- Theta or apex angle 126 degree (even better penetration)
- Theta or apex angle 120 degree (even better penetration)
- Theta or apex angle 115 degree (deceleration increases and have less speed at 750 mm depth as compared to case 4 so rebound)



Figure 5.29: formation of Tungsten EFP in void (pictures in zoomed form)(at 20,30,40,50,80 μ sec)

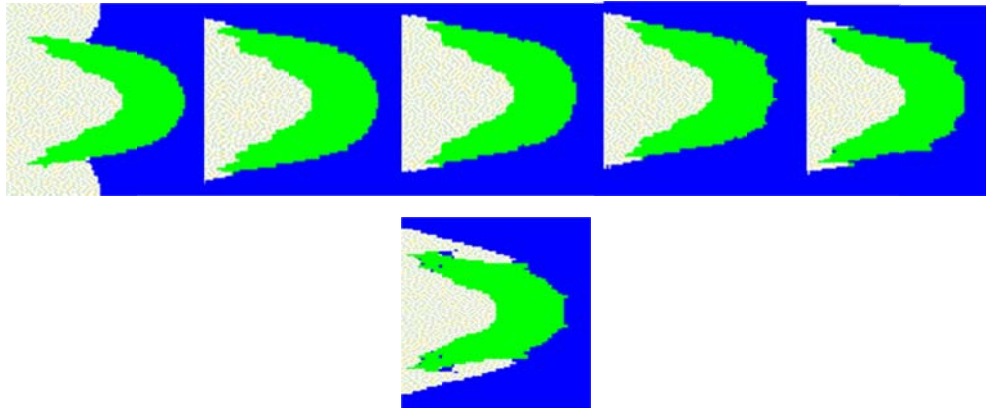


Figure 5.30: formation of Tungsten EFP in Water

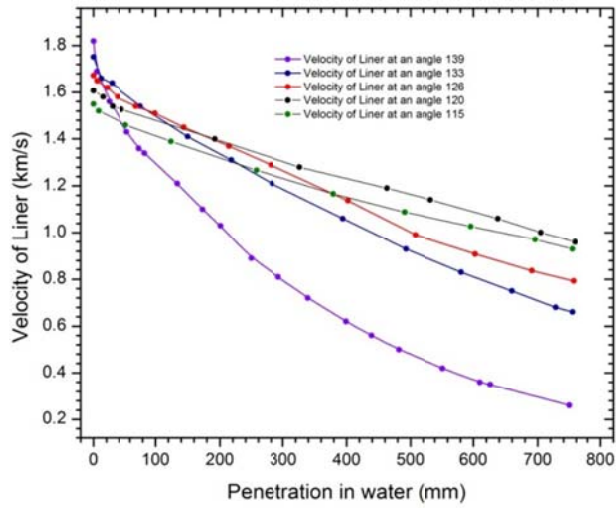


Figure 5.31: Optimization of curvature of Tungsten-EFP in water

As it is seen from fig 5.31 and table 4 the best results are for angle 120°.

Table 5.4: Effects of Liner curvature on EFP performance

Liner Curvature degree	Stable Velocity(km/s)	Velocity after 750mm penetration in water(km/s)
139	1.82	0.26
133	1.75	0.65
126	1.68	0.80
120	1.61	0.96
115	1.55	0.92

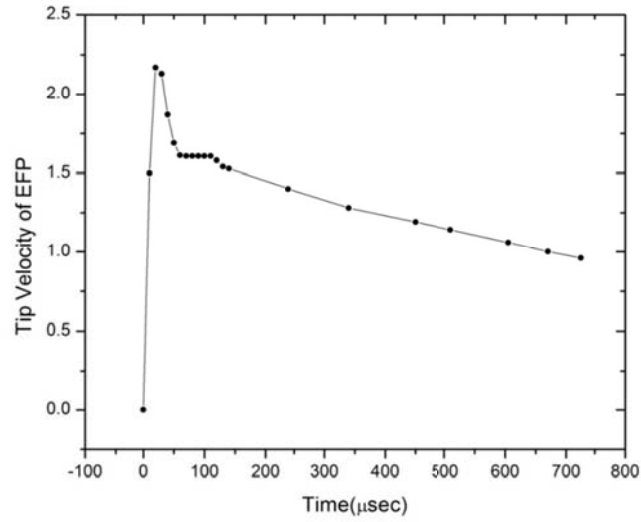


Figure 5.32: Velocity profile of optimized Tungsten-EFP in water

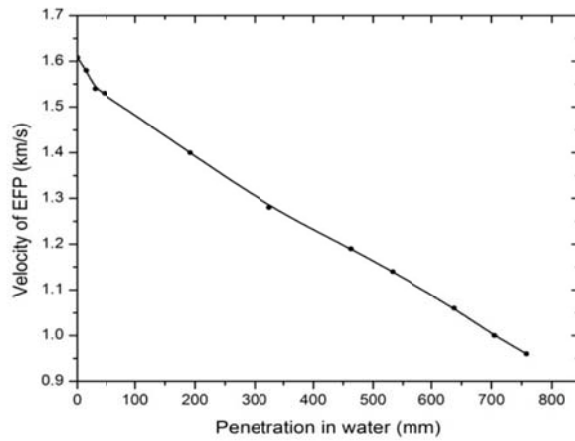


Figure 5.33: Velocity profile of optimized Tungsten-EFP in water

Here case 4 have the highest penetration capability in water or lesser deceleration. Only 40% reduction in speed after 13 CD distance in water. It covers 21CD distance in water

as its velocity decreases from 1.61 to 0.55km/s as seen from figure 5.33.the equation of linear fit is given by

$$V = 1.57528 - 0.0008214X$$






Where ‘X’ is the penetration distance in water at any time ‘ V’ is the velocity of EFP at that time.

Table 5.5 comparison of penetration distance in water when EFP has velocity 0.55km/s

Thickness	Material	Shape	Stable velocity	Instantaneous velocity	Penetration in water
2mm	Copper	Elongated	2.06	0.55	2.5CD
3.0-----2.0	Copper	W-shaped	1.72	0.55	4.0CD
3.5----0.5	Copper	Heart shaped	1.63	0.55	8.3CD
2mm	Tungsten	U-shaped	1.601	0.55	21CD

In above table velocity in km/s. the penetration is increased to about 240% as compared to reference results in case of copper liner designs. In case of tungsten made liner the penetration is increased to about 90% as compared to reference results [24].

Table 5.6: Effects of different explosives on EFP shape, velocity and L/D Ratio

Type	Density (kg/cm ³)	Detonation velocity(km/s)	Shape	L/D at stable Velocity	Tip Velocity(km/s)
HMX	1.891	9.11		1.077	1.61
Octal	1.821	8.48		1.037	1.57
Comp B	1.717	7.98		0.800	1.45
PBX9407	1.600	7.91		0.720	1.41
TNT	1.630	6.93		0.550	1.23

HMX explosive shows larger L/D ratio and highest Tip velocity.

5.7 EFFECT OF MOVING WATER ON EFP PERFORMANCE

If water moving against EFP with velocity less than 100 times that of EFP then after 12CD distance in water , its velocity reduces to 5% more than in still water

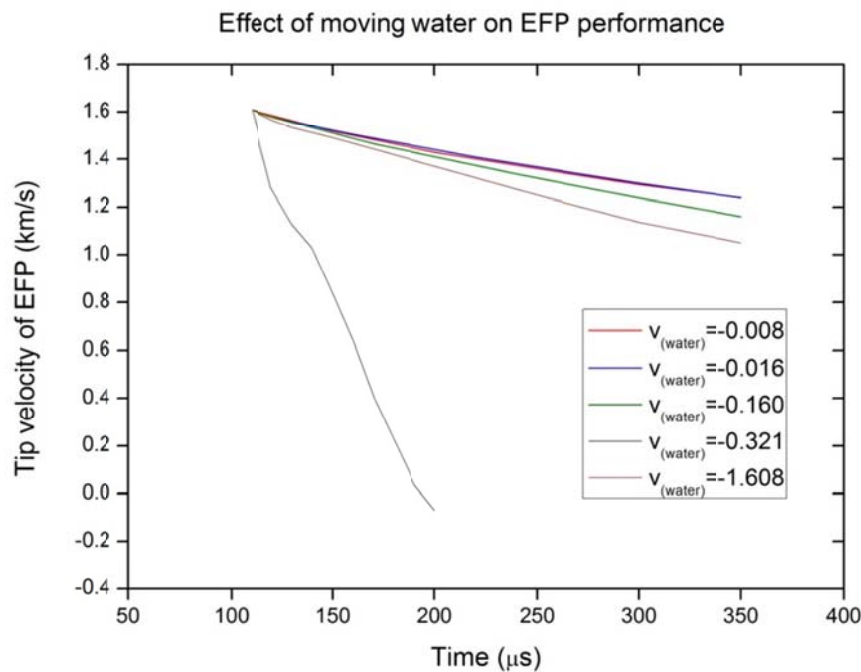


Figure 5.34: Behavior of velocity of water on Tungsten EFP penetration in water

If water moving against EFP with velocity equal to that of EFP then after 1CD distance only in water , its velocity becomes negative and it eroded and breaks into pieces. If water moving against EFP with velocity less than 5 times (in our case=-0.3216) that of EFP then after 350usec penetration in water its velocity decreased to 15% that of EFP in still water at that time. If water moving against EFP with velocity less than 10 times (in our case=-0.1608) that of EFP then after 350usec penetration in water its velocity decreased to 6.5% that of EFP in still water at that time. If water moving against EFP with velocity less than 100 times or more less than that of EFP then after 350usec

penetration in water its velocity decreased to only less than 2-3% that of EFP in still water at that time. so we concluded that in our case (for this design) in normal river or sea water speed there will be no change in speed of EFP.

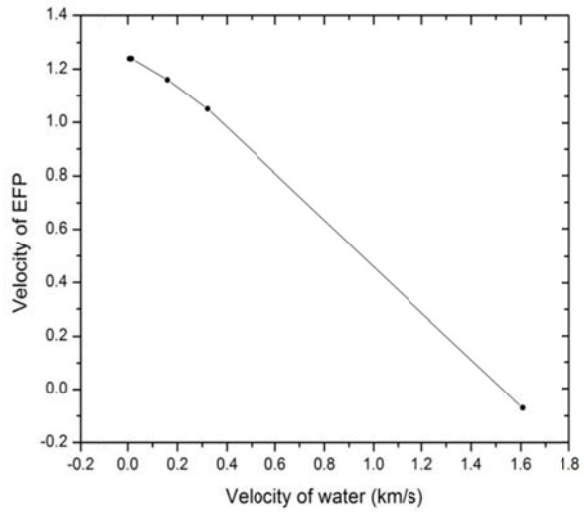


Figure 5.35: Effect of velocity of water on Tungsten EFP penetration in water

5.8 SUMMARY AND CONCLUSIONS

1. The final shape and velocity of an explosively formed projectile (EFP) is very sensitive to its initial parameters like liner curvature, liner thickness, liner type (uniform thickness or contour type), explosive type, etc.
2. By optimizing Liner thickness stability and penetration can be increased
3. Uniform thickness EFPs (in case of copper liner) eroded rapidly, while contour types liner shows less erosion of mass and hence some better penetration through water. In this case efficiency is increased to 240% than reference results.
4. Liner material play very important role in the performance of EFP especially under water copper made liners show poor performance, while tungsten liner shows much better penetration and no erosion of mass as well.
5. 90% increase in penetration in water as compared with reference results in case of tungsten liner
6. Of all the available explosives HMX shows better results as it has higher density and detonation velocity.
7. Normal river speed water not affecting the EFP performance.

5.9 RECOMMENDATIONS

1. Validation of simulation results by experiments
2. Effect of Moving water with different directions on EFP performance
3. 3D simulation
4. Wave shaping concept for better efficiency

References

1. "Commercial High Explosives" URL: <http://www.fireandsafety.eku.edu/VFRE-99/Recognitioin/High/high.htm> - 41k
2. Carleone, J., (ed), "Tactical Missile Wareheads", Vol 155, Progress in Astronautics and Aeronautics, AIAA, Washington, DC, 1993.
3. Walters, W. P. and Zukas, J. A., "Fundamentals of Shaped Charges", CMC Press, Balimore, USA, 1998.
4. Zukas, J. A. and Walters, W. P. S, J. A., "Explosive Effects and Applications", Springer, New York, USA, 2003.
5. Cooper, P.W., "Explosive Engineering", Wiley-VCH, New York, 1996.
6. Mader, C. L., "Numerical Modeling of Explosives and Propellants", CRC Press, New York, 1998.
7. Hartmann, M., "Behind Armour Debris- Numerical Simulation A Literature Review", FOI Swedish Defense Agency Report, Tumba, 2005.
8. Ansys Autodyn V 11.0, Manual by Century Dynamics. (AUTODYN Theory manual, Revision 4.3, Century Dynamics).
9. Cook R. D., Malkus D. S. and Plesha M. F., "Concept and Applications of Finite Element Analysis", Third edition, John Wiley & Sons 1989, ISBN 0471-84788-7
10. PAPPU S., MURR L. E. "Hydrocode and Micro-Structural Analysis of Explosively formed Penetrators", Journal of Materials Science, 37 (2002) 233 - 248 (University of Texas at EI Paso USA, Kluwer Academic Publishers 2002).
11. Scheffler, D. R. and Zukas J. A., "Practical Aspects of Numerical Simulation of Dynamic Events: Material Interfaces", International Journal of Impact Engineering 24 (2000) 821 - 842.
12. Wisstein E. W., "Finite Volume Method", From Math World. URL: <http://mathworld.wolfram.com/FiniteVoluteMethod.html>McQueenD., "Compendium of

- Results From Firing Different Explosively Formed Projectiles", DSTO Systems Sciences Laboratory, Australia, 2003, DSTO-TR-1479.
13. Davies, N., "Ammunition Technology Handbook", Ammunition Systems and Explosives Technology Department, RMCS, Cranfield University, 2001.
 14. Erfeng, A., Zhaowu S., Tingqing Z. & Derun W. "Application Study on A Shaped Charge Warhead", Proc. of International Autumn Seminar on Propellants, Explosives and Pyrotechnics, Guilin, China, October 15-18, 2003.
 15. Katatama M., Takeba A., Toda S., and Kibe S., "Analysis of Jet Formation and Penetration by Conical Shaped Charge with the Inhibitor", International Journal of Impact Engineering 23 (1999) 443 - 454.
 16. Borne, B., K., Cowan G. and Curtis J. P., "Shape Charge Warheads Containing Low Melt Energy Metal Liners", Proc. of the 19th International Symposium on Ballistics, Switzerland, 2001.
 17. Hermann, J.W., Pehrson G. R., and Berus, E. R., "Experimental and Analytical Investigation of Self Forging Fragments for the Defeat of Armor at Long Standoff", Proc. of the 3rd International Symposium on Ballistics, to write
 18. Meyers, M. A. "Dynamic Behavior of Materials", John Wiley & Sons, Inc., New York, 1994.
 19. Chick, M and Hatt D. J., "The Mechanism of Initiation of Compo B by a Material Jet", Proc. of the 7th International Symposium on Detonation, Naval Surface Weapons Center, MP 82- 334, p353, 1981
 20. Chick M and Bussell T. J., Frey R. B. & al, "Jet Initiation Mechanism and Sensitiveness of Covered Explosives", Proc. of the 9th International Symposium on Detonation, OCNR 113291-7, p. 14104, 1981.
 21. J. O. HALLQUIST, User's Manual for DYNA2D - An Explicit Two-Dimensional Hydrodynamic Finite Element Code with Interactive Rezoning, Report UCID-18756, Lawrence Livermore National Laboratory, 1980.
 22. Zernow L: Proc. 10th International Symposium on Ballistics, San Diego, 1987.
 23. Janzon B, Chick M and Bussell T: Proc. of 14th International Symposium on Ballistics, Cubec City, Canada, 1993.

24. C.Lam and D.McQueen., "Study of Penetration of Water by an Explosively Formed projectile", Weapons System Division Aeronautical and Maritime Research Laboratory, DSTO-TR-0686
25. N.M. Burman, G.M. Weston, "The modelling of High Strain Rate Deformation and Penetration Problems Using Finite Element Analysis", Report, AD-A268 653, Defense Technical Information Center, DTIC, Melbourne, Victoria, Australia, 1993
26. Cartright, M ,Simpson,P.J. Non-solid explosives for shaped charges III: Metal liner devices used in explosive ordinance disposal operations, journal of energetic materials, 1545-8822, Volume 27, Issue, 3, page 166-185.
27. Chick, M.C. Bussel, T, J, Frey, R, B, An influence of explosive geometry on shaped charge jet performance, journal of energetic materials, 1545-8822, Volume 5, Issue 3, 1987, page 327-342.
28. Waker, F.E, Wasley, R, J, Critical energy for shock initiation of heterogeneous explosives. Explosivstoffe, 17:9, 1969.
29. Lee, P.R, Critical power density: A universal quantitative initiation of criterion. 10th International symposium on ballistics, VI II, 27-29 October, San Diego, California, 1987 explosives
30. Zhang, X. Chen, H., Zhao, Y, Numerical simulation of shelled explosive initiated by EFP. Journal of ballistics, Vol 18 No. 1, pp. 838-844
31. Doig, A. Introduction to shaped charge, RMCS, MSc Notes, p2-4, 2000.
32. Christman, D.R., Gehring, J.W., Journal of applied physics, vol. 37, pp 1579-1587, 1996
33. Doyle, J.R., Buchholz, R.L, Design, development, fabrication, and testing program to demonstrate the feasibility of the mass focus fragmentation warhead, Honeywell technical report, AFATL-TR-72-187, September, 1973.
34. Holer, V., Stilp, A.J., Penetration of steel and high density rods in semi-infinite steel targets, 3rd International symposium on ballistics, Karlsruhe, 23-25 March 1977.